Earth-Science Reviews 204 (2020) 103180

Contents lists available at ScienceDirect

Earth-Science Reviews

journal homepage: www.elsevier.com/locate/earscirev

The Late Triassic Extinction at the Norian/Rhaetian boundary: Biotic evidence and geochemical signature

Manuel Rigo[a,b,*], Tetsuji Onoue[c], Lawrence H. Tanner[d], Spencer G. Lucas[e], Linda Godfrey[f], Miriam E. Katz[g], Mariachiara Zaffani[a], Kliti Grice[h], Jaime Cesar[h], Daisuke Yamashita[c], Matteo Maron[a,i], Lydia S. Tackett[j], Hamish Campbell[k], Fabio Tateo[b], Giuseppe Concheri[l], Claudia Agnini[a], Marco Chiari[b], Angela Bertinelli[m]

[a] Department of Geosciences, University of Padova, Via G. Gradenigo 6, 35131 Padova, Italy
[b] IGG-CNR (Istituto di Geoscienze e Georisorse), Padova, Firenze, Italy
[c] Department of Earth and Planetary Sciences, Kyushu University, Fukuoka 819-0355, Japan
[d] Department of Biological and Environmental Sciences, Le Moyne College, Syracuse, NY 13214, USA
[e] New Mexico Museum of Natural History and Science, 1801 Mountain Road NW, Albuquerque, NM 87104, USA
[f] Department of Earth and Planetary Sciences, Rutgers University, Piscataway, NJ 08854, USA
[g] Department of Earth and Environmental Sciences, Rensselaer Polytechnic Institute, 110 8th St., Troy, NY 12180, USA
[h] Western Australian Organic and Isotope Geochemistry Centre, The Institute for Geoscience Research, School of Earth and Planetary Science, Curtin University, GPO BOX U1987, Perth, WA 6845, Australia
[i] Department of Earth Sciences, University of Milan, Via L. Mangiagalli 34, 20133 Milan, Italy
[j] Department of Geosciences, North Dakota State University, Dept. 2745, Fargo, ND 58108-6050, USA
[k] GNS Science, 1 Fairway Drive, Avalon, Lower Hutt, Wellington 5010, New Zealand
[l] Department of Agronomy Food Natural Resources Animals and Environment (DAFNAE), University of Padova, Viale dell'Università, 16, 35020 Legnaro, Italy
[m] Department of Physics and Geology, University of Perugia, Via A. Pascoli, 06123 Perugia, Italy

ARTICLE INFO

Keywords:
Mass extinction
$\delta^{13}C_{org}$
Norian
Rhaetian
Late Triassic
LIPs
Meteorite crater

ABSTRACT

The latest Triassic was an interval of prolonged biotic extinction culminating in the end-Triassic Extinction (ETE). The ETE is now associated with a perturbation of the global carbon cycle just before the end of the Triassic that has been attributed to the extensive volcanism of the Circum-Atlantic Magmatic Province (CAMP). However, we attribute the onset of declining latest Triassic diversity to an older perturbation of the carbon cycle ($\delta^{13}C_{org}$) of global extent at or very close to the Norian/Rhaetian boundary (NRB). The NRB appears to be the culmination of stepwise biotic turnovers that characterize the latest Triassic and includes global extinctions of significant marine and terrestrial fossil groups. These biotic events across the NRB have been largely underappreciated, yet together with a coeval disturbance of the carbon cycle were pivotal in the history of the Late Triassic. Here, we present new and published $\delta^{13}C_{org}$ data from widespread sections (Italy, Greece, ODP, Australia, New Zealand, USA, Canada). These sections document a previously unknown perturbation in the carbon cycle of global extent that spanned the NRB. The disturbance extended across the Panthalassa Ocean to both sides of the Pangaean supercontinent and is recorded in both the Northern and Southern Hemispheres. The onset of stepwise Late Triassic extinctions coincides with carbon perturbation ($\delta^{13}C_{org}$) at the NRB, indicating that a combination of climatic and environmental changes impacted the biota at a global scale. The NRB event may have been triggered either by gas emissions from the eruption of a large igneous province pre-dating the NRB, by a bolide impact of significant size or by some alternative source of greenhouse gas emissions. As yet, it has not been possible to clearly determine which of these trigger scenarios was responsible; the evidence is insufficient to decisively identify the causal mechanism and merits further study.

1. Introduction

The Triassic Period is unique among the geologic periods of the Phanerozoic because it is the only period constrained by two of the largest declines in biodiversity of the Phanerozoic: 1) the end-Permian mass extinction, which is the most extensive biotic extinction of the

* Corresponding author at: Department of Geosciences, University of Padova, Via G. Gradenigo 6, 35131 Padova, Italy.
E-mail address: manuel.rigo@unipd.it (M. Rigo).

https://doi.org/10.1016/j.earscirev.2020.103180
Received 28 August 2019; Received in revised form 4 April 2020
Available online 13 April 2020

Phanerozoic (e.g., Benton and Twitchett, 2003; Erwin, 2006); and 2) the end-Triassic biotic decline, culminating in the extinctions across the Triassic/Jurassic boundary (TJB; e.g., Hallam, 2002; Tanner et al., 2004; Richoz et al., 2007; Lucas and Tanner, 2018).

Environmental instability is characteristic of the Triassic. During the Late Triassic in particular (ca. 237–201.3 Ma), Pangaea experienced a variable climate regime (e.g., Preto et al., 2010; Rigo et al., 2012a; Trotter et al., 2015) that was interrupted by several global events including humid episodes (e.g., Carnian Pluvial Episode, Late Triassic of Simms and Ruffell, 1989, 1990; Simms et al., 1995) and warm cycles. The warm cycles (W1, W2, and W3) are documented by $\delta^{18}O_{phosp}$ from conodont biogenic apatite (Rigo et al., 2012a; Trotter et al., 2015) and supported by pCO_2 reconstruction based on stable isotopes of pedogenic carbonates from the Newark Basin in the USA (Knobbe and Schaller, 2018). Additional evidence of climatic perturbations at the NRB has been suggested recently by evidence of a major mega-monsoon climate in Australian paleolatitudes. In fact, Zeng et al. (2019) describe a mega-monsoon climate for the Northwest Shelf of Australia that reached its peak during the Carnian Pluvial Episode and weakened at the NRB, so that the climate during the Rhaetian became non-seasonal. This change in seasonality also was expressed by changes in vegetation as indicated by certain plant biomarkers from the same region (e.g., cadalene and retene: Cesar and Grice, 2019). These climatic perturbations may have resulted from extreme volcanic activity, with consequent impacts on Earth's biota (e.g., Raup and Sepkoski, 1982; McElwain et al., 1999; Hallam, 2002; Marzoli et al., 2004; Rigo et al., 2007; Rigo and Joachimski, 2010; McRoberts et al., 2008; Lucas, 2010; Ogg, 2012; Dal Corso et al., 2014; Trotter et al., 2015).

Important clues to the evolution of ocean water chemistry, oxygenation, and productivity of past marine environments, including those of the Triassic, are recorded by changes in the isotopic composition of sediments (organic and inorganic). In particular, perturbations observed in $\delta^{13}C$ values are widely applied and interpreted as indicators of paleoclimatic and paleoenvironmental changes (e.g., Hayes et al., 1999; Veizer et al., 1999; Payne et al., 2004; Ward et al., 2004; Korte et al., 2005; Lucas, 2010; Muttoni et al., 2004, 2014; Galli et al., 2005, 2007; Mazza et al., 2010; Preto et al., 2010; Whiteside and Ward, 2011; Zaffani et al., 2017, 2018). The stable carbon isotope record available for the Triassic gives a general overview of the evolution of $\delta^{13}C$, but its paleoclimatic and paleooceanographic interpretation is somewhat uncertain due to the multiple ecological and geochemical controls that can drive changes in the stable carbon isotope system.

From a broad perspective, a pronounced negative $\delta^{13}C$ excursion across the Permian/Triassic boundary marks the beginning of the Triassic Period. This severe perturbation of the global carbon cycle is followed by large isotopic variability during the earliest Triassic (e.g., Payne et al., 2004; Tanner, 2010) that eventually leads to a more stable period spanning the Middle to the early Late Triassic (Julian, early Carnian) (Payne et al., 2004; Tanner, 2010). This interval is characterized by steadily rising $\delta^{13}C$ values that are likely related to biotic recovery in the aftermath of the end-Permian mass extinction and the resulting enhanced storage of organic carbon in terrestrial environments (e.g., Lucas, 2010).

The Late Triassic is framed by two significant negative carbon isotope shifts, both linked to the emplacement of Large Igneous Provinces (LIPs). The first $\delta^{13}C$ excursion occurred during the middle Carnian climate perturbation referred to as the Carnian Pluvial Episode (Dal Corso et al., 2014, 2018) and is likely associated with the emplacement of the Wrangellia Igneous Province (e.g., Furin et al., 2006; Dal Corso et al., 2014). The second $\delta^{13}C$ perturbation, recorded at the Triassic-Jurassic transition (uppermost Rhaetian to lowermost Hettangian), is associated with the End-Triassic Extinction (ETE) and the emplacement of the Central Atlantic Magmatic Province (CAMP; e.g., Marzoli et al., 2004; Whiteside et al., 2010; Schaller et al., 2012; Zaffani et al., 2018).

The causes of the Triassic carbon isotope excursions remain a topic of much debate, with the most likely trigger mechanisms being related to greenhouse gas emissions produced by volcanic activity, the volatiles of which can derive from both the magma itself and/or be released by the combustion of crustal materials in contact with the magma (Clapham and Renne, 2018). Alternatively, other processes that can contribute to the occurrence and magnitude of the observed carbon cycle perturbation include changes in primary biotic productivity, global ocean anoxia or seafloor methane release (e.g., Richoz et al., 2007; Lucas, 2010; Clapham and Renne, 2018). In principle, all of these processes are capable of perturbing the global carbon cycle and causing episodes of biotic crises (e.g., Rampino and Stothers, 1988; Wignall, 2001; Jones and Jenkyns, 2001; Ward et al., 2004; Richoz et al., 2007; van de Schootbrugge et al., 2008; Jenkyns, 2010; Tanner, 2010; Pálfy et al., 2001; Trotter et al., 2015).

Published $\delta^{13}C_{org}$ data are especially focused on mass extinction events (i.e., Permian/Triassic boundary, Triassic/Jurassic boundary), whereas long-term background data (before and after those events) are comparatively less abundant. Data from the Norian (ca. 227.0–205.7 Ma; Diakow et al., 2011, 2012; Maron et al., 2015) of North America reveal rapid oscillations of $\delta^{13}C_{org}$ that culminate in a positive $\delta^{13}C_{org}$ peak, which corresponds to the virtual extinction of the bivalve *Monotis* around the NRB (Ward et al., 2004; Wignall et al., 2007; Whiteside and Ward, 2011; Rigo et al., 2016; Bertinelli et al., 2016; Zaffani et al., 2017). This positive excursion has been interpreted as the possible result of reduced circulation of ocean waters (Sephton et al., 2002; Ward et al., 2004; Wignall et al., 2007), and it is preceded by a negative shift (Maron et al., 2015; Rigo et al., 2016; Bertinelli et al., 2016; Zaffani et al., 2017).

Relatively few $\delta^{13}C_{org}$ records are available for the Rhaetian (ca. 205.7–201.3 ± 0.2 Ma; Williford et al., 2007; Schoene et al., 2010; Wotzlaw et al., 2014; Maron et al., 2015; Rigo et al., 2016), a stage marked by significant faunal turnovers in both the marine and continental realms, including taxa such as ammonites (Guex et al., 2004; Whiteside and Ward, 2011), conodonts (Kozur and Mock, 1991; Giordano et al., 2010; Karádi et al., 2019), bivalves (McRoberts and Newton, 1995), radiolarians (Carter, 1993; Ward et al., 2001; Carter and Hori, 2005; O'Dogherty et al., 2010), the coral reef community (Flügel and Kiessling, 2002), dinoflagellates and foraminiferans (Hesselbo et al., 2002), calcareous nannofossils (van de Schootbrugge et al., 2007; Preto et al., 2012, 2013), theropod dinosaurs (Olsen et al., 2002), and terrestrial plants (McElwain et al., 1999, 2009; Kürschner et al., 2007; Bonis et al., 2009; Cesar and Grice, 2019). The Rhaetian experienced a series of biotic crises and turnovers that culminated in the crisis at the Triassic/Jurassic boundary (TJB), which supports the hypothesis of a step-like extinction pattern for the end-Triassic mass extinction (e.g., Hallam, 2002; Tanner et al., 2004; Whiteside and Ward, 2011; Lucas and Tanner, 2018; Karádi et al., 2019).

Moreover, the latest Rhaetian is widely accepted to have been affected by the extensive eruptive activity of the CAMP, which is thought to have triggered three major negative carbon isotope excursions (CIEs): the 'main' CIE at the TJB, preceded by the late Rhaetian 'initial' and 'precursor' CIEs; the latter two are commonly associated with two different eruptive phases of the Moroccan CAMP (Marzoli et al., 2004; Hesselbo et al., 2002, 2007; Deenen et al., 2010; Zaffani et al., 2018). Although much attention has been focused on $\delta^{13}C$ evolution across the TJB, much less is known about the background carbon isotope conditions from the Norian (aside from the aforementioned North American section) to the early-middle Rhaetian and their possible links to the faunal extinction patterns and/or climate events documented at this time.

Herein we present evidence of a significant $\delta^{13}C_{org}$ excursion at the NRB. A key section representing this excursion is the Pignola-Abriola section (GSSP candidate for the Rhaetian Stage) (Lagonegro Basin, Southern Apennines, Italy; Fig. 1), which is a sedimentary NRB succession deposited in the western portion of the Tethys Ocean (Bazzucchi et al., 2005; Rigo et al., 2016; Bertinelli et al., 2016). We compare carbon isotope data from this site with data from other sections located

Section area	Palaeogeographic position				Lithostratigraphy		Stratigraphic sections				Biostratigraphy														
	Northern Emisphere	Southern Emisphere	Western Tethys	Eastern Tethys	lithostratigraphic units	lithologies of the lithostratigraphic units	section name	geographic coordinates (datum WGS 84)	lithologies of the stratigraphic sections	Norian/Rhaetian Boundary	conodonts	radiolarians	bivalves	ammonoids	nannoplancton	dinoflagellates	palynomorphs	ostracods	benthic foraminifers	brachiopods	gastropods	echinoderm fragments	plant debris	icnofossils
Lagonegro Basin (Southern Apennines - Italy)	x		x		2. Scisti Silicei Fm (e.g., radiolarites) (Latest Norian/late Rhaetian to Late Jurassic)	cm-thick cherts, radiolarites and siliceous shale beds	Pignola-Abriola section	40° 33′ 23.50″ N, 15° 47′ 1.71″ E	1(upper part). limestones (sometimes silicified) alternating with dark grey shales and thin black cherty beds	shaley with repetitive, thin and well-laminated interbeds of black shale	x	x*												
									1(lower part). thin-bedded, cherty limestones (sometimes dolomitized), with thin layers of shale and calcarenite		x	x*												
					1b. Transitional interval, if present (Calcari con Selce Fm) (Sevatian 1)	red clay horizon; black and grey, well laminated, shaley levels, rich in organic matter	Mt. Volturino section	40° 24′ 13.46″ N, 15°49′ 2.25″ E	2. shales and radiolarites, with a few calcarenitic intercalations		x	x												x
									1b. 3-metre-thick red clay horizon; black and grey, well laminated, shaley levels, rich in organic matter, above the red horizon	black and grey shaley levels, rich in organic matter	x	x*												
					1a. Calcari con Selce Fm (i.e., Cherty Limestones) (Carnian to latest Norian/late Rhaetian)	cherty limestones intercalated with marls, siltstones and calcarenites	Madonna del Sirino section	40° 07′ N, 15° 48′ E	2. red and green, radiolarian-bearing siliceous shales, cherts and scattered calcarenites	dark shales and cherts, rich in radiolarians	x	x												x
									1b. 3-metre thick red clay horizon		x	x**												
									1a. well-bedded micritic limestones, with cherty nodules and layers		x	x**												
# Pindos Zone (Peloponnese, Greece)	x		x		Drimos Fm (late Carnian to Early Jurassic)	cherty limestones intercalated with shales; calcirudites; radiolarian cherts and radiolarites	Kastelli section	07° 54′ N, 22° 02′ E	limestones with thin-shelled bivalves and chert nodules, alternating with shales; calcirudites and redeposited limestones. Radiolarian cherts and radiolarites in the upper part, are locally intercalated with thin argillaceous limestones	limestones with red cherty layers or radiolarites	x		x	x											
# Wombat Basin (northwestern Australia, ODP Site 761C)		x		x	core 26R (Norian-Rhaetian)	dark limestones with calcareous claystone interbeds		16° 44.23′ S, 115° 32.10′ E								x	x	x	x					
					cores 29R to 27R	oxidized conditions (no organic materials)												x	x					
					cores R32 to R30 (Norian-Rhaetian)	calcareous sediments				black claystones					x			x	x				x	
					core R33 (Late Norian)	clayey siltstone				black claystones						x							x	
# Carnarvon Basin, Dampier sub-Basin (North-West Australia)		x		x	2. Brigadier Fm (Rhaetian)	very thin shaley/sandy layers interbedded with several medium to fine sandstones	Delambre-1 well	18° 31′ 05″ S, 116° 41′ 48″ E								x	x							
					1. Mungaroo Fm (Norian)	mostly shaley with fine-grained dark claystone, and thin coal layers	North Ranking-5 well	19° 34′ 18.82″ S, 116° 09′ 30.42″ E								x	x							
# Murihiku Terrane - Zealandia (New Zealand)		x		x	Newcastle Group: 2. Ngutunui Fm (Norian-Rhaetian)	volcaniclastic rocks are dominated by fine sandstone and siltstone, with minor but conspicuous conglomerates, tuffs and shell beds; no limestones	Kiritehere section	38° 31.16′ S, 174° 71.01′ E	2. shales	shales			x	?						x	x		x	x
					1. Arawi Shellbeds Fm (Norian)				1. shales and thin sandstones, with shell beds (bivalves coquina)				x	?						x	x		x	x
# Nevada, USA	x			x	Nun Mine Member (Gabbs Fm) (late Norian-Rhaetian)	b. carbonate-and-shale (upper section) a. shale-and-carbonate (lower section)	New York Canyon section	38° 49.69 N, 118° 08.27 W		carbonate-and-shale section, a few of meters above the top of the shale and carbonate unit	x		x	x							x	x		
British Columbia, Canada	x			x	Sandilands Fm (late Norian? Rhaetian to Early Jurassic)	grey thinly-bedded siliceous siltstone with minor sandstone, limestone and shale; limestone lenses and concretions and volcaniclastic material	Kennecott Point section			dark grey thinly-bedded siliceous siltstone	x	x	x	x					x*					x

unpublished data

* mostly pyritized

** poorly preserved/calcified

Fig. 1. Geological setting scheme of the studied sections.

at varying latitudes and from both hemispheres, and we associate the $\delta^{13}C_{org}$ perturbations across the NRB with heightened faunal turnovers, including ammonoids, conodonts, radiolarians, bivalves, coral reefs, and terrestrial and marine vertebrates.

2. Geological setting of the studied sections

We have examined and correlated multiple stratigraphic sections situated in the two hemispheres, on opposite sides of Pangea, and located at different latitudes by using chemo- and biostratigraphic constraints (Fig. 1).

In particular, we studied three NRB sections that crop out in the Southern Apennines (Italy) in the Lagonegro Basin, which is considered a branch of the western Tethys Ocean and part of the Ionian Sea (Ciarapica and Passeri, 1998; Stampfli et al., 2003) (Fig. 2). In the Lagonegro Basin, the Upper Triassic is represented by the Calcari con Selce (i.e., Cherty Limestones) and the overlying Scisti Silicei (e.g., radiolarites) formations. The Calcari con Selce Formation consists of limestones with cherts in nodules and beds, intercalated with marls and siltstones (rare calcarenites), and rich in conodonts, radiolarians and thin-shelled pelagic bivalves (e.g., *Halobia, Monotis*) (e.g. Amodeo, 1999; Bazzucchi et al., 2005; Bertinelli et al., 2005, 2016; Giordano et al., 2010; Rigo et al., 2012b, 2016) (Fig. 1). The three sections, Pignola-Abriola, Mt. Volturino and Madonna del Sirino, document a well-exposed and fairly complete NRB, and they have been investigated from stratigraphic, sedimentological and biostratigraphic points of view (e.g. Amodeo, 1999; Bertinelli et al., 2005, 2016; Bazzucchi et al., 2005; Reggiani et al., 2005; Rigo et al., 2005, 2012a, 2016; Giordano et al., 2010, 2011) and also for magnetostratigraphy (Pignola-Abriola, Maron et al., 2015, 2019), geochemistry (Amodeo, 1999; Casacci et al., 2016) and chemostratigraphy (Trotter et al., 2015; Zaffani et al., 2017) (Fig. 1). Another section from the western Tethys Ocean is the Kastelli section (Pindos Zone) that is exposed in the Peloponnese (Greece) (Degnan and Robertson, 1998), and belonging to the tectono-stratigraphic terranes of the Hellenides (Brunn, 1956). This section consists of cherty limestones alternating with shale, with documented slumps (Drimos Formation), and bears conodonts, foraminifers, and thin-shelled bivalves belonging to the genus *Halobia* (Degnan and Robertson, 1998) (Fig. 1). Both the Lagonegro Basin and Pindos Zone were located in the Northern Hemisphere during the Late Triassic (Fig. 2). The Kennecott Point (British Columbia) and the New York Canyon (Nevada) sections were also located in the Northern Hemisphere during the Norian-Rhaetian time interval, but on the western side of Pangea, facing the Panthalassa Ocean (Fig. 2). The Kennecott Point section (Queen Charlotte Islands, British Columbia, Canada) is represented by black calcareous siltstone and shale, rich in fossils (e.g. bivalves, radiolarians), sometimes in bivalve coquina beds, belonging to the Peril Formation (e.g. Ward et al., 2001, 2004), and deposited in a back-arc basin (Cameron and Tipper, 1985; Carter, 1993). The New York Canyon section was also deposited in a back-arc basin before being accreted onto the western United States (Nevada), and it is represented by the two facies of the Nun Mine Member and Mount Hyatt Member of the Gabbs Formation, which are the offshore slope facies in the shale-and-carbonate succession, and a combination of nearshore facies, both

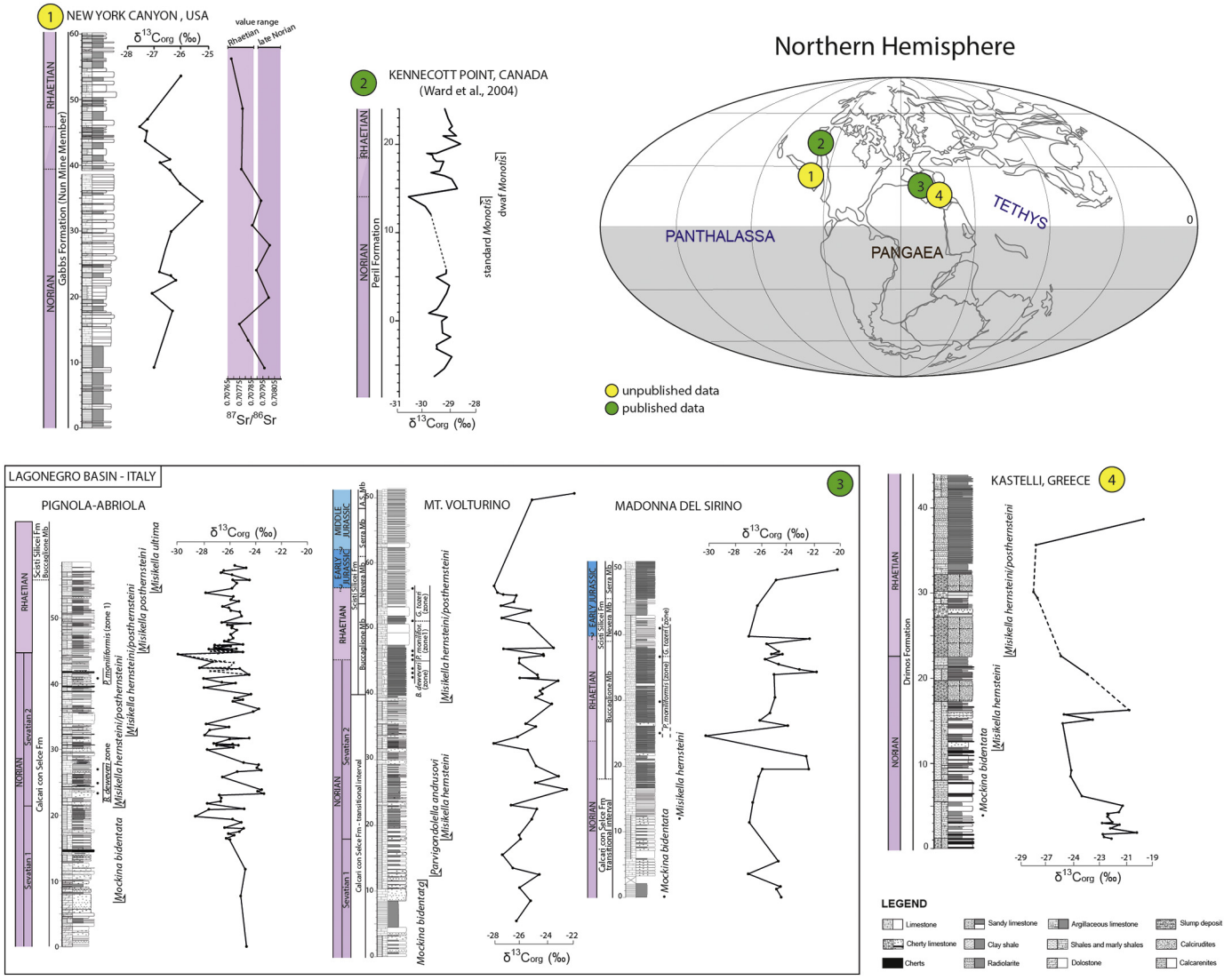

Fig. 2. Position of the studied sections in the Northern Hemisphere. 1) Lithostratigraphy and Sr isotope ratio for the New York Canyon section (Nevada) are after Tackett et al. (2014). The $\delta^{13}C_{org}$ is illustrated here for the first time. 2) Information of the Kennecott point section is from Ward et al. (2004). 3) Litho-, bio- and chemostratigraphy of the Lagonegro sections (Pignola-Abriola, Mt. Volturino and Madonna del Sirino) are from Zaffani et al. (2017 and references herein). Dashed line in Pignola-Abriola represents $\delta^{13}C_{org}$ new data (modified after Zaffani et al., 2017). 4) Kastelli section (Greece) is illustrated with new litho-, bio- and chemostratigraphic data. Dashed lines in $\delta^{13}C_{org}$ indicate gaps due to slumps.

above and below fair-weather wave base in the carbonate-and-shale unit (Laws, 1982; Tackett and Bottjer, 2016) (Fig. 1, 2).

The studied sections from the North-West Shelf of Australia (Wombat and Carnarvon Basins) and New Zealand (Murihiku Terrane) were instead located in the Southern Hemisphere (southern Tethys) at that time, although at different paleolatitudes, i.e. 25–30° S for the North-West Shelf, Australia (Exon and von Rad, 1994) and close to the South Pole for the New Zealand section (Seton et al., 2012) (Figs. 1, 3). The Triassic strata of Hole 761C (core R33 to R26) from the Wombat Basin are dominated by black clayey siltstone at the base, and layers of calcareous sediments above, representing a proximal slope and evolving into an inner shelf to reefal carbonate margin. These cores of the Ocean Drilling Program (ODP) have been constrained biostratigraphically with dinoflagellate cysts, forams and nannofossils (Bralower et al., 1992; Brenner et al., 1992; Zaninetti et al., 1992; Gardin et al., 2012) (Figs. 1, 3). The Northern Carnarvon Basin received instead a thick fill of fluvio-deltaic sediments during a long-term regression. The predominant lithology corresponds to claystone and sandstone, with siltstone and some coal interbedded in the Mungaroo Formation (Norian), whereas claystone becomes more dominant in the overlying Brigadier Formation (Rhaetian), where the depositional environment had a major estuarine influence. Both formations are dated by palynomorphs (Woodside Energy Ltd., 1977; Hocking et al., 1987; Longley et al., 2002) (Figs. 1, 3). The Kiritehere section crops out on the western Tasman Sea coast of the central North Island (New Zealand), and it consists of a volcaniclastic sedimentary rock succession with slumps dominated by fine sandstone and siltstone rich in bivalve coquinas (Arawi Shellbeds Formation), grading into thin siltstones and shales (Ngutunui Formation), rich in bivalves (Grant-Mackie, 1981, 2013). This succession is interpreted to represent a mid-shelf environment that accumulated in an elongate forearc basin marginal to an active, subduction-related volcanic arc that lay to the west of Kiritehere, along the edge of Gondwana (Grant-Mackie, 2013) (Figs. 1, 3).

3. Geochemistry – materials and methods

3.1. Methods for $\delta^{13}C_{org}$ of bulk organic matter

Prior to acidification, all samples were washed in high-purity water and selected to avoid sampling of unrepresentative portions (e.g.,

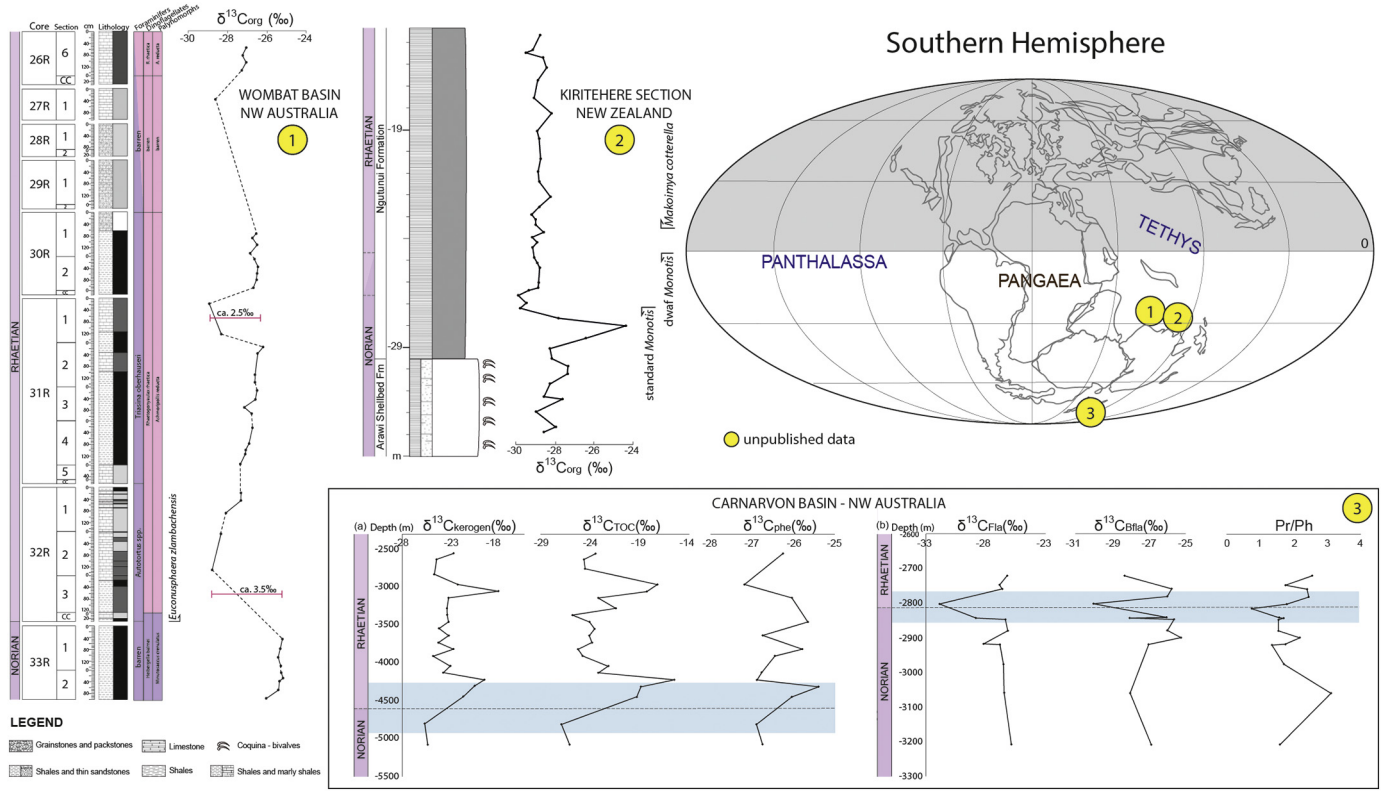

Fig. 3. Position of the studied sections in the Southern Hemisphere. 1) Norian-Rhaetian interval at Site 761C hole C (Wombat Basin, NW Australia), with nannofossils distribution from Gardin et al. (2012), forams from Zaninetti et al. (1992), and dinoflagellates from Brenner et al. (1992). Dashed lines in $\delta^{13}C_{org}$ indicate gaps in core recovery. 2) Lithostratigraphy, selected bivalve bioevents and δ^{13}Corg of the Kiritehere section, North Island, New Zealand. 3) Evidence of isotopic perturbations in wells from the Northwest Shelf of Australia. a) $\delta^{13}C$ values for the kerogen, total organic carbon content (TOC) and phenanthrene (Phe) for source rock samples from the Delambre-1 well in the Dampier sub-Basin. b) $\delta^{13}C$ of fluoranthene (fla), benzofluoranthenes (Bfla) and pristane (Pr)/phytane (Ph) ratios for source rock samples from the North Rankin - 5 well in the Dampier sub-Basin. $\delta^{13}C$ of fluoranthene from Cesar and Grice (2017). Norian-Rhaetian boundary from Woodside Energy Ltd. (1981) and Marshall and Lang (2013). $\delta^{13}C$ data from the Delambre-1 well from Marshall and Lang (2013).

fracture-filling mineralization, bioturbation, diagenetic alteration). A few grams of each sample were reduced to a fine powder using a Retsch RM0 grinder or manually, using an agate mortar, and dried overnight at 40 °C. All the pulverized rock samples were then acid-washed with 10% HCl overnight (at least 12 h). Successively, the solution was discarded after centrifuging. Samples were then neutralized in deionized water, dried at 40°C overnight and wrapped in tin capsules.

The $\delta^{13}C_{org}$ analyses were undertaken using a Delta V Advantage mass spectrometer connected to a Flash HT Elemental Analyzer. For every set of analyses, multiple blank capsules and isotope standards (IAEA CH-6 = -10.45‰, IAEA CH-7 = -32.15‰) (Coplen et al., 2006) were included. Raw data were corrected for the blank contribution and then were calibrated against IAEA CH-6 and IAEA CH-7 following the two-point calibration method. The standard deviation of the in-house standard ($\delta^{13}C_{org}$ = -26.00‰) during the period of analyses was better than 0.2‰.

The $\delta^{13}C_{org}$ analyses refer to the $\delta^{13}C$ composition of bulk organic matter. Organic matter can be made up of a number of components, such as bacteria, phytoplankton, zooplankton, pollen and/or other terrestrial biomass. Each of these components has a characteristic value of $\delta^{13}C_{org}$. As a result, changes in relative contributions of these components could affect the $\delta^{13}C_{org}$ record, without necessarily requiring changes in the isotopic composition of the ocean and/or the atmosphere (Van de Schootbrugge et al., 2008; Fio et al., 2010; Bartolini et al., 2012). Nevertheless, if similar coeval trends occur at distant locations, the robust correlation between $\delta^{13}C_{org}$ excursions can indicate regional, or, if more extensive, global interpretation. In fact, the amplitude and absolute values of coeval $\delta^{13}C_{org}$ changes may be amplified or dampened by local environmental conditions and source control, i.e., the contribution of marine relative to terrestrial organic matter, and profound changes in the composition of standing biomass, i.e., the terrestrial floras or phytoplankton communities (Van de Schootbrugge et al., 2008). Despite regional differences in absolute value, the similarity between two or more coeval trends in the $\delta^{13}C_{org}$ profile likely indicates a regional or global history (Bartolini et al., 2012).

3.2. Compound specific isotope analysis (CSIA)

The aromatic compounds were isolated by small-scale silica gel liquid chromatography, dissolved in *n*-hexane (see also Maslen et al., 2011), and analysed by compound specific isotope analyses. A Thermo Scientific Trace GC Ultra connected to a Thermo Scientific Delta V Advantage irMS via a GC Isolink and Conflo IV was used for the stable carbon compound specific isotope analysis (CSIA) by gas chromatography – isotope-ratio mass spectrometry (GC-irMS). For each fraction, 1 μL of solution was injected into a split-splitless injector that operates in splitless mode, held at 280 °C. The compounds were separated chromatographically on a wall-coated open tubular (WCOT) fused silica capillary column (60 m X 0.25 mm internal diameter) with a 0.25 μm 5% phenyl-methyl-silicon stationary phase (DB-5). The temperature of the GC oven was programmed from 40 to 325 °C (at 3 °C/min) and was held isothermally for 45 minutes at 325 °C. Compound identification was achieved by comparing the mass spectra and the available literature. Helium was used as the carrier gas at a constant flow of 1.5 mL/min. GC column outflow passed through the GC Isolink combustion reactor (copper oxide and nickel oxide, held at 1000 °C), which combusted each peak to a separate peak of CO_2. The $\delta^{13}C$ values are expressed in parts per mil (‰) relative to the International Vienna Peedee

Belemnite (VPDB) standard and were calculated by Thermo Isodat software from the integration of the 44, 45 and 46 mass ion currents. For every two sample measurements, a mixture of standards with known $\delta^{13}C$ values was analysed in order to ensure instrument accuracy. Peaks co-eluting, as well as those at very low concentrations, were not considered for our interpretations. Only target compounds with a standard deviation of less than 0.4‰ were taken into account.

Kerogen and total organic carbon (TOC) $\delta^{13}C_{org}$ values were measured in a Delambre-1 well using a 20/20 ion ratio mass spectrometer and Roboprep preparation system, manufactured by Europa PDZ, UK. Ground samples were placed in a tin capsule and dropped onto a furnace at 1000 ˚C while in an oxygen atmosphere. Combustion products were passed through a second furnace (600 ˚C) where excess oxygen was absorbed, and nitrogen oxide was reduced to nitrogen. The samples were also passed over magnesium perchlorate to trap the water. The system was calibrated using known $\delta^{13}C$ international laboratory standards (Grice et al., 2005).

4. Results

4.1. Lagonegro Basin, Pignola-Abriola section

A total of 14 new samples were prepared and analyzed to augment the organic carbon $\delta^{13}C$ set across the NRB. The results are consistent with the samples analysed previously for the same time interval, fitting the $\delta^{13}C_{org}$ curve presented in Zaffani et al. (2017) and illustrated in Fig. 2. Values for the Mt. Volturino and Madonna del Sirino sections are those reported in Zaffani et al. (2017) (Fig. 2) (Table S1).

4.2. Pindos Zone (Peloponnese, Greece), Kastelli section

Only 30 of the 99 samples collected from this section provided a $\delta^{13}C_{org}$ signal; the carbon content of the remaining samples was too low for carbon isotope analysis. Therefore, the resolution of the $\delta^{13}C_{org}$ profile is lower than expected, but some trends can be outlined and may be related to the biostratigraphic data. The $\delta^{13}C_{org}$ curve depicts three trends corresponding to portions of the three perturbations (S1, S2 and S3) described by Zaffani et al. (2017). These are, in ascending stratigraphic order: i) a decrease through the conodont *Mockina bidentata* Zone below the FO of *Misikella hernsteini* Zone (ca. 6‰) that was interpreted as equivalent to S1 (Zaffani et al., 2017); ii) a positive trend within the *Misikella hernsteini* Zone, representing the return to positive values of the S2 recorded in the Lagonegro Basin (Zaffani et al., 2017); and iii) a negative shift starting in the upper *M. hernsteini* Zone and intersecting the FO of *Misikella posthernsteini*, corresponding to the S3 negative shift (Zaffani et al., 2017) (Fig. 2) (Table S1).

4.3. Nevada – USA, New York Canyon section

Eighteen shale samples were analysed to describe the variation of the $\delta^{13}C_{org}$ across the NRB in the New York Canyon section, though we note that the position of the NRB in the New York Canyon section is not tightly constrained by current biostratigraphy. The resulting $\delta^{13}C_{org}$ profile shows a negative CIE coinciding with the negative $^{87}Sr/^{86}Sr$ shift documented within the Mount Hyatt Member of the upper Gabbs Formation (Tackett et al., 2014). These trends are similar to those recorded in other coeval sections (Korte et al., 2003). In the lower part of the section, a general trend towards more positive $\delta^{13}C_{org}$ values is documented; this trend ends with a $\delta^{13}C$ value of ca. -25‰. Subsequently, a $\delta^{13}C$ depletion of ca. 2.5‰ is recorded, with a successive return to more positive values (Fig. 2) (Table S1).

4.4. Wombat Basin (northwestern Australia), ODP SITE 761C

A total of 25 shale samples (and rare shaley marls) from cores 33 (Section 1-2), 32 (1, 2, 3) and 31 (3, 4, 5) collected during the ODP were analysed. Despite the low core recovery at Hole 761C, a decrease in the $\delta^{13}C_{org}$ profile of ca. 3.5‰ at the Norian-Rhaetian transition was detected and was placed between 32R and 33R by the occurrence of the typical Rhaetian nannofossil *Euconusphaera zlambachensis* in core 32R Section 3 (Gardin et al., 2012) (Fig. 3) (Table S1).

4.5. Murihiku Terrane – Zealandia (New Zealand), Kiritehere section

The 34-metre thick Kiritehere section was studied in great detail. Sixty-eight samples of shales and thin siltstones from the upper part and bivalve coquinas from the lower part were collected and analysed for organic stable carbon isotopes ($\delta^{13}C_{org}$). In the lower part of the section, a severe negative shift of ca. 5‰ was detected, preceded by a short positive peak with respect to background values of ca. -28‰. The NRB is placed between the $\delta^{13}C_{org}$ negative shift and the disappearance of the bivalve *Monotis*. It is noteworthy that the $\delta^{13}C_{org}$ curve after the NRB perturbation follows rapid positive-negative oscillations (Fig. 3) (Table S1).

4.6. Dampier sub-Basin, Carnarvon Basin, North-West Australia

A core from the Delambre-1 well demonstrates a trend of depleted isotopic values for the kerogen and total organic carbon, just below the NRB (Fig. 3). The recovery follows a positive excursion, and subsequently, the isotopic profiles become more stable. We also investigated the $\delta^{13}C$ of select polycyclic aromatic hydrocarbons (PAHs) such as phenanthrene and source-specific PAHs, including fluoranthene and benzofluoranthenes, which are combustion products from land plants (Jiang et al., 1998; Grice et al., 2007; Cesar and Grice, 2017). Phenanthrene shows depleted $\delta^{13}C$ values (comparable with the $\delta^{13}C$ of kerogen and TOC) at the NRB in the Delambre-1 well, even though this signal might be overprinted by multiple sources (marine and terrestrial) of this compound. However, if we consider source specific compounds, i.e., fluoranthene and benzofluoranthenes, the negative isotope excursion is more evident in a core from the North Rankin-5 well, immediately above the NRB. In the North Rankin-5 well, these isotopic trends are corroborated by a record of anoxia (isoprenoids ratio Pristane/Phytane $<$ 1) (Fig. 3) (Table S1).

5. Discussion

5.1. Extinction record across the NRB

Here we review the nature of extinctions that took place across the NRB and during the early-middle Rhaetian. Most of these extinctions were long conflated as a single mass extinction at the end of the Triassic, the so-called ETE at the TJB (e.g., Sepkoski Jr., 1982, 1996; Olsen and Sues, 1986; Olsen et al., 1987; Kiessling et al., 1999, 2007; Tomašových and Siblík, 2007; Wignall et al., 2007; Vazquez and Clapham, 2017). However, recent developments in marine (e.g., McRoberts, 2010; O'Dogherty et al., 2010; Orchard, 2010; Rigo et al., 2018) and non-marine biostratigraphy, magnetostratigraphy (e.g., Muttoni et al., 2010; Kent et al., 2017; Maron et al., 2019), radioisotopic dating (e.g., Wotzlaw et al., 2014; Davies et al., 2017) and other dating methods (e.g. Maron et al., 2015) have allowed a much more detailed sequencing of biotic events during the NRB and TJB intervals than was possible 20 years ago (cf. Hallam, 2002; Tanner et al., 2004; Lucas and Tanner, 2008, 2015, 2018). These developments enable the identification of significant extinctions of marine pelagic biota across the NRB and during the Rhaetian, and the interpretation of tetrapod extinctions on land across the same boundary.

Nevertheless, we add the caveat that better stratigraphic resolution is needed for many of the taxa across the NRB. Thus, some of the extinctions at the NRB identified here are likely subject to the compiled correlation effect, meaning that there may be within-late Norian or within-Rhaetian events that are condensed into an apparent, single NRB

extinction. Thus, further work is needed to better resolve the timing of some biotic events across the NRB. Nonetheless, we do believe that there is a strong signal, and that there were substantial extinction events across the NRB, here referred to as the NRB extinction.

5.1.1. Marine extinctions across the NRB.

In the marine realm, there were striking and extensive extinctions among several biotic groups across the NRB, almost all of which were members of marine pelagic communities. Most striking, and long known, are the ammonoid extinctions. It has long been clear that the largest extinction of Late Triassic ammonoids took place at the end of the Norian, not at the end of the Triassic (Kummel, 1957; House, 1963; Kennedy, 1977; Newell, 1967; Teichert, 1988; Whiteside and Ward, 2011; Lucas, 2018a). After this extinction, only a few ammonoid taxa populated the Rhaetian seas, limited to heteromorphs and some Arcestaceae and Clydonictacea (Wiedmann, 1973). The Late Triassic ammonoid extinctions were a succession of diversity drops, with the last, most substantial drop at the end of the Norian, not at the end of the Triassic. Thus, ammonoid extinctions across the TJB are best described as stepwise (Wiedmann and Kullman, 1996; Lucas, 2018a).

A compilation of ammonoid global diversity at the stage level indicates that, after a Norian (mostly Alaunian) peak in diversity, the most substantial extinction of ammonoid families and genera took place across the NRB (Lucas, 2018a). This is best documented in the New York Canyon area of Nevada, USA, where Taylor et al. (2000, 2001), Guex et al. (2002, 2003), and Lucas et al. (2007) plotted ammonoid distribution based on decades of collecting and study. Their work documents a two-phase latest Triassic ammonoid extinction, one extinction phase in the late Norian followed by a phase of low diversity Rhaetian ammonoid fauna that became extinct by the end of the Triassic (also see Lucas and Tanner, 2008, 2018). Thus, the ammonoid extinction across the NRB is profound and evident in both abundance data and stratigraphic ranges.

Recent analysis of marine bivalve diversity across the TJB, based on a generic compilation at the stage level, shows that generic diversity peaked during the Norian and was followed by a sharp drop into the Rhaetian and Hettangian (Ros, 2009; Ros and Echevarria, 2011; Ros et al., 2011, 2012). Extinction rates were high during the Rhaetian, and origination rates were low. This is consistent with more detailed studies (local and regional) of Late Triassic marine bivalve stratigraphic distributions (e.g., Allasinaz, 1992; McRoberts, 1994; McRoberts and Newton, 1995; McRoberts et al., 1995; Wignall et al., 2007). The latter studies identified multiple and selective bivalve extinction events within the Norian, Rhaetian, and across the TJB, with a particularly important extinction at the NRB. This extinction of bivalves included the virtual disappearance of the cosmopolitan and abundant pectinacean *Monotis* (Dagys and Dagys, 1994; Hallam and Wignall, 1997) including the two dwarf Rhaetian species (McRoberts, 2007; Krystyn et al., 2007; McRoberts et al., 2008). McRoberts' (2007, 2010) summaries of the Late Triassic diversity dynamics of 'flat clams' (halobiids and monotids) indicate these organisms suffered their largest extinction at the NRB. Allasinaz (1992) also drew attention to the end-Norian turnover of megalodontid bivalves and concluded that the marine bivalve extinction at the NRB was larger than the extinction at the TJB, during which megalodontids decreased in size before their extinction (Todaro et al., 2017, 2018).

A major turnover in radiolarians took place across the TJB, and this has been widely considered as an important component of a marine mass extinction. Like the ammonoid and bivalve extinctions, this 'mass extinction' also has important components that precede the TJB. Global compilations indicate a substantial drop in radiolarian generic diversity from the Norian into the Rhaetian (e.g., O'Dogherty et al., 2010; Kiessling and Danelian, 2011). At the best-studied and most complete radiolarian record across the TJB (Queen Charlotte Islands in western Canada, recently renamed Haidi Gwaii), Carter (1993, 1994) established the *Proparvicingula moniliformis* Zone and the *Globolaxtorum tozeri* Zone to encompass the lower and upper Rhaetian radiolarian assemblages. Over half of the 160 radiolarian species present at the base of the *P. moniliformis* Zone disappear by the top of this zone; this is a substantial within-Rhaetian radiolarian extinction (Longridge et al., 2007). Biostratigraphic ranges of 156 radiolarian species in the Triassic deep-sea sections from Japan show a dramatic increase in extinction rates in the end-middle Norian following the Manicouagan impact event (Hodych and Dunning, 1992; Ramezani et al., 2005), and during the late Rhaetian (Onoue et al., 2016).

Conodonts also underwent substantial extinctions across the NRB. Micropaleontologists have long known that the Late Triassic witnessed a stepwise decline in conodont diversity as extinction rates were relatively high and origination rates were low (e.g., Clark, 1980, 1981, 1983; Sweet, 1988; Kozur and Mock, 1991; Aldridge and Smith, 1993; De Renzi et al., 1996). The single largest Late Triassic extinction of conodonts took place during the Carnian (at the Julian/Tuvalian boundary) when nearly all platform conodonts disappeared (Rigo et al., 2007, 2018; Rigo and Joachimski, 2010). Conodont diversity recovered somewhat through the Norian to decline again into the Rhaetian. Within the Rhaetian, nearly all conodont taxa disappeared before the TJB, with only one or two taxa found in the youngest Rhaetian conodont assemblages (Mostler et al., 1978; Kozur and Mock, 1991; Orchard, 2003, 2010; Orchard et al., 2007; Bertinelli et al., 2016; Rigo et al., 2016; Du et al., 2020). Karádi et al. (2019) show Rhaetian conodont diversity dynamics as a stepwise extinction of four genera.

In the aftermath of the end-Permian extinctions, the Triassic was a time when the marine fish fauna changed from the chondrichthyan-rich faunas of the late Paleozoic to the actinopterygian-dominated fish faunas of the Mesozoic-Cenozoic (e.g., Romano et al., 2013). The Late Triassic saw the diversification of neopterygian actinopterygians, and the origin of durophagous feeders. A global compilation by Romano et al. (2013) suggests that marine fish generic diversity dropped from the Norian into the Rhaetian, but the records of Norian fish fossils from Lagerstätten and the absence of similar deposits from the Rhaetian (cf. Tintori and Lombardo, 2018) make it difficult to determine if the diversity drop is real or an artifact of preservation and hence collection bias.

Similarly, marine reptiles show an 'evolutionary bottleneck' across the NRB (Renesto and Dalla Vecchia, 2018). This is represented by a diversity crash among the ichthyosaurs and the extinction of the thalattosaurs and the tanystropheids. However, like the fish record, the marine reptile record is affected by biases, particularly the general reduction of shallow marine platforms during the Rhaetian, which were the preferred habitats and sites of fossil preservation of the marine reptiles. Thus, the evolutionary bottleneck of marine reptiles across the NRB may in part reflect this bias (Renesto and Dalla Vecchia, 2018).

The extinctions in the reef community at the end of the Triassic are best documented in the Tethys, where the reef ecosystem collapsed at the end of the Triassic; carbonate sedimentation nearly ceased, and earliest Jurassic reefal facies are rare (see Lucas and Tanner, 2018 and references cited therein). However, whether this was a global event remains unclear. Notably, Stanley et al. (2018) presented a compelling analysis that shows a reduction in corallite integration across the TJB, which is a morphological simplification in response to environmental stress similar to that seen in the ammonoids and radiolarians across the TJB (cf. Guex, 2016). Clearly, the reef crisis in the Tethys began at the end of the Norian when the scleractinian coral reefs (which produce planktotrophic larvae today) reached their peak of diversity, structural complexity and distribution, to diminish through the Rhaetian to a sudden collapse at the TJB (e.g., Kiessling et al., 1999; Kiessling, 2001; Flügel, 2002; Flügel and Kiessling, 2002). There was also an extinction of most microbial reefs and of algal reefs across the NRB (Flügel and Senowbari-Daryan, 2001).

In conclusion, significant extinctions took place in the marine realm across the NRB, particularly among ammonoids, bivalves, radiolarians and conodonts. Similar extinctions likely took place among

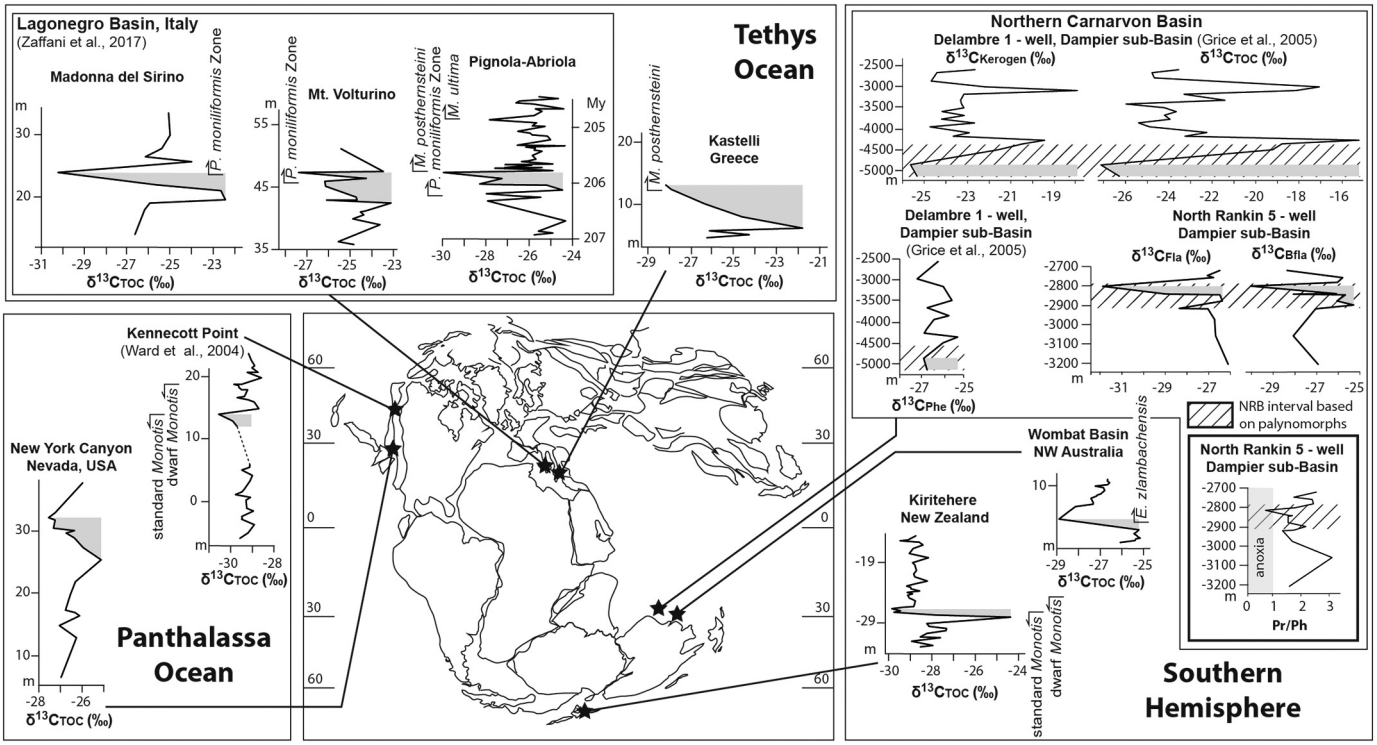

Fig. 4. Chemostratigraphic profiles of Norian/Rhaetian boundary. Paleomap of Pangea during the NRB (Late Triassic) with localities and $\delta^{13}C_{org}$ curves cited in the text. The Norian/Rhaetian boundary constraints are illustrated for each section. Grey areas indicate the global $\delta^{13}C_{org}$ negative shift.

actinopterygian fishes, marine reptiles and in the reef community, though their records suffer from problems of taphonomy, facies and provinciality that make these extinctions more difficult to interpret.

5.1.2. Terrestrial extinctions across the NRB.

Evaluating terrestrial extinctions across the NRB has long been confounded by the difficulty of identifying and correlating the base of the Rhaetian in non-marine sections (e.g., Lucas and Tanner, 2007; Kozur and Weems, 2010; Lucas et al., 2012; Lucas and Tanner, 2015). Nevertheless, the extinctions that took place across the NRB in the terrestrial realm do not appear to have been extensive or sudden. Land plants, both palynomorphs and megaflora, show no significant extinction across the NRB (e.g., Barbacka et al., 2017; Lucas and Tanner, 2018; Kustatscher et al., 2018), though there were diversity crashes of local and regional extent. These are best seen in the palynological record in Western Europe and in the Newark Supergroup in eastern North America where many vessicate palynomorphs disappear during the late Norian or at the NRB (Lucas and Tanner, 2007, 2015 and references cited therein). However, the broad significance of these events remains to be demonstrated, and we are not able to correlate them to any turnover in the megaflora.

There is no evidence of terrestrial arthropod extinctions across the NRB. Indeed, diverse analyses of the fossil record of insects detect no evidence of a diversity crash during the Late Triassic or across the TJB (Clapham and Karr, 2012; Condamine et al., 2016; Grimaldi and Engel, 2005; Karr and Clapham, 2015; Labandeira, 2005; Labandeira and Sepkoski Jr., 1993). Grimaldi and Engel (2005, p. 73) concluded, "there seems to have been little differentiation between insect faunas of the Late Triassic and Early Jurassic".

The record of terrestrial tetrapods does indicate some turnover across the NRB. Most of the large temnospondyl amphibians were extinct by the end of the Norian, with capitosaurs disappearing just before the NRB (Lucas, 2018b). Among reptiles, two groups of herbivores – the rhynchosaurs and dicynodonts – that had been significant components of Middle Triassic-Carnian tetrapod communities, became extinct late in the Norian (Spielmann et al., 2013; Racki and Lucas, 2018). The traversodontid cynodonts, a diverse group of Gondwanan synapsid herbivores, also disappeared at or just before the NRB (Abdala and Gaetano, 2018).

The classic concept of a TJB tetrapod extinction was largely predicated on the disappearance of the 'thecodonts,' subsequently referred to as the crurotarsans and more specifically (during the Late Triassic) encompassing the rauisuchians, aetosaurs and phytosaurs. Rauisuchians became extinct during the late Norian, aetosaurs were of low diversity after the NRB and became extinct during the Rhaetian or at the TJB, and phytosaur diversity crashed across the NRB although they apparently survived at low diversity across the TJB (Maisch and Kapitzke, 2010; Lucas and Heckert, 2011; Lucas and Tanner, 2015; Lucas, 2018b). Therefore, we can only interpret some turnover in the terrestrial tetrapods, and mostly late Norian extinctions or NRB diversity crashes. These are parts of a stepwise extinction of tetrapod taxa across the TJB that presaged the dinosaur-dominated terrestrial communities of the Jurassic-Cretaceous (Lucas, 2018b).

In brief, the evidence for a terrestrial extinction across the NRB is limited. Some tetrapod groups went extinct between the late Norian and late Rhaetian, and there are some local turnover events in the palynofloral record across the NRB. The significance and synchroneity of these events merits further study, particularly to calibrate their timing more precisely.

5.2. Correlation and magnitude of CIE

In the uppermost Norian sections, multiple $\delta^{13}C_{org}$ perturbations are associated with increases in bulk sediment TOC at locations ranging from the western Tethys (Rigo et al., 2016; Zaffani et al., 2017) to the Panthalassa Ocean (Ward et al., 2001).

Immediately below the NRB, which is defined by the first occurrence of the conodont *Misikella posthernsteini* (Krystyn, 2010; Rigo et al., 2016; Bertinelli et al., 2016; Zaffani et al. 2017), a negative $\delta^{13}C_{org}$ excursion of up to 5 ‰ occurs at three localities in the western Tethys

(Pignola-Abriola, Mt Volturino and Madonna del Sirino sections in the Lagonegro Basin). Intra-basinal $\delta^{13}C_{org}$ correlations rely on integrating biostratigraphy (conodonts, radiolarians) to obtain time-constrained successions for comparisons. As a result, the $\delta^{13}C_{org}$ decrease across the Norian-Rhaetian transition is a feature identified as common to all studied sections of the Lagonegro Basin (Fig. 4).

It is noteworthy that the three Lagonegro Basin sections document the $\delta^{13}C_{org}$ negative shift at the NRB from different lithologies (Zaffani et al., 2017), as the Lagonegro Basin was progressively falling below the CCD during the latest Triassic to Early Jurassic (e.g., Amodeo, 1999; Bertinelli et al., 2005; Rigo et al., 2012b), thereby demonstrating that the excursions are not a diagenetic artifact (Jiang et al., 2019). Moreover, the $\delta^{13}C_{org}$ negative trend documented at the NRB at these three Lagonegro Basin localities was also identified in another Tethyan site, the Kastelli section, which crops out in the Pindos Zone, on the Peloponnese Peninsula of Greece (Kafousia et al., 2011) (Fig. 4), thus extending the correlation within the western Tethys. Of greater importance, this event is not limited to the Tethys, but occurs also in western Canada at Kennecott Point (British Columbia) (Ward et al., 2001, 2004; Whiteside and Ward, 2011) and at the New York Canyon section, Nevada (USA), both of which were located on the far side of the Panthalassa Ocean during the Late Triassic (Fig. 4).

This CIE is also now documented in Southern Hemisphere sections, including the Dampier sub-Basin (Northern Carnarvon Basin) on the Northwest Shelf of Australia (Grice et al., 2005, 2007; Cesar and Grice, 2017) and for the first time in the Wombat Basin (NW Australia, ODP Site 761C, Core 33R-32R-31R) and the Kiritehere section (North Island of New Zealand), the latter of which was located at a high latitude during the Late Triassic (Fig. 4). In the Northern Carnarvon Basin, the most depleted $\delta^{13}C$ values of kerogen and TOC are recorded just below the NRB in the Delambre-1 well (Fig. 4), followed by more positive $\delta^{13}C$ values. This positive $\delta^{13}C_{org}$ peak was also identified in British Columbia, close to the near extinction of the bivalve *Monotis* (Ward et al., 2004; Wignall et al., 2007; Whiteside and Ward, 2011), and interpreted as the result of a slowing of ocean circulation with a consequent decrease in oxygenation (Sephton et al., 2002; Ward et al., 2004). The $\delta^{13}C$ was measured in select polycyclic aromatic hydrocarbons (PAHs) from the Northern Carnarvon Basin, such as phenanthrene (Delambre-1 well), and source-specific PAHs, such as fluoranthene and benzofluoranthenes (North Rankin-5 well). Importantly, these compounds are produced by the combustion of land plants (Jiang et al., 1998; Grice et al., 2007; Cesar and Grice, 2017), and both exhibit a negative CIE excursion at or immediately above the NRB (Fig. 4) as defined by palynomorphs, thereby correlating the events from the marine and terrestrial realms. The amplitude and values of the $\delta^{13}C_{org}$ curves differ among the different basins due to variations in the type of organic matter, but the similarity of the $\delta^{13}C_{org}$ curves suggests an event of global extent (Fig. 4).

Based on the profiles presented here (e.g., Lagonegro Basin), a short positive excursion from background $\delta^{13}C_{org}$ values is documented at the base of the radiolarian *Proparvicingula moniliformis* Zone (uppermost Norian), followed by the rapid onset of a significant negative shift that lasted ca. 1 Myr (Maron et al., 2015), and ended close to the base of the Rhaetian (= LO of conodont *M. posthernsteini*) (Rigo et al., 2016; Bertinelli et al., 2016; Zaffani et al., 2017). This negative shift in $\delta^{13}C_{org}$ is also associated with the virtual disappearance of the cosmopolitan, standard-sized pelagic bivalve *Monotis* (Ward et al., 2004) (Fig. 4). Following this negative shift, the $\delta^{13}C_{org}$ curve recovers quickly as a positive peak to near background for ca. 300 k.y. (Pignola-Abriola section), or slightly more negative values (e.g., Southern Hemisphere sections). This is followed by a chaotic interval that is characterized by short oscillations in $\delta^{13}C_{org}$ and the presence of small (also referred to as dwarf) species of the bivalve *Monotis*. At the base of this chaotic interval, the standard-sized *Monotis* disappears, but the perturbation of the system persisted until the stabilization that is observed at the FO of the conodont *M. ultima* (Zaffani et al., 2017) (Fig. 4).

5.3. Potential causes of the CIE

The worldwide low $\delta^{13}C_{org}$ interval associated with a strong faunal turnover at the NRB likely resulted from multiple mechanisms that may have included some combination of decreased primary productivity, enhanced magmatic activity and outgassing (including pyrogenic volatiles), dissociation of clathrates, thermal degradation of peatland, and/or input of ^{12}C from an extraterrestrial object, any of which may potentially create a global signal (e.g., Kent et al., 2003; Jenkyns, 2010; Schaller et al., 2012; Meyers, 2014; Zaffani et al., 2017; Clapham and Renne, 2018). We thus propose that a large volume of ^{13}C-depleted CO_2 entered the ocean-atmosphere system just before the NRB (grey area in Fig. 4).

Although the impact of a large extraterrestrial object has not been proposed as a cause of the NRB extinction, such an event could have produced the negative shift of $\delta^{13}C_{org}$, reflecting consequent decreased primary productivity (D'hondt et al., 1998). The largest impact known for the Late Triassic formed the 90-km diameter Manicouagan structure (Spray et al., 2010), but repeated dating of the structure by various methods has consistently yielded middle Norian ages (Hodych and Dunning, 1992; Ramezani et al., 2005; van Soest et al., 2011; Clutson et al., 2018), nearly 10 million years prior to the NRB (Fig. 5). The radioisotopically constrained U-Pb age of 205.7 Ma for the NRB (Wotzlaw et al., 2014) is close to radiometric ages from melt rock at the Rochechouart impact crater (< 50 km diameter) in south-central France; Schmieder et al. (2010) provided an $^{40}Ar/^{39}Ar$ age of 203 ± 2 Ma (recalculated to the decay constants of Renne et al., 2011), and Cohen et al. (2017) presented an $^{40}Ar/^{39}Ar$ age of 206.92 ± 0.20/0.32 Ma (Fig. 5). However, geochemical evidence of the iron meteorite impactor (Tagle et al., 2009) combined with the lack of carbonate-rich target rocks (Lambert, 2010) suggests that the volume of climatically active gases (e.g., CO_2) released from the impact site would not have had an appreciable environmental effect that could have triggered the NRB extinction. Moreover, there have been no reports of impact debris (shock-metamorphosed quartz, melt-glass spherules or anomalous levels of Ir) associated with NRB sections. Hence, we discount the likelihood of a bolide impact as the driver of the NRB environmental event.

The concentration of marine extinctions at the NRB in the pelagic realm (planktonic, nektonic, benthic) suggests that the negative $\delta^{13}C_{org}$ excursion records decreased productivity. Although the largest known impacts (e.g., Chicxulub) are considered capable of disrupting the trophic system by blocking photosynthetically active radiation (PAR), the Rochechouart structure was produced by an impactor nearly an order of magnitude too small to have been effective on a global scale. Thus, eruption of a LIP, with resultant outgassing, seems a far more likely candidate. As has been suggested for the TJB, large-scale volcanic outgassing is capable of producing short-term temperature reductions, due to the effects of sulfuric acid (H_2SO_4) aerosols formed from outgassed sulphur dioxide (SO_2), followed by longer-term warming forced by increased atmospheric pCO_2 (Tanner et al., 2004; Lucas and Tanner, 2018).

Previous workers have documented global-scale drops in both the $^{87}Sr/^{86}Sr$ and $^{187}Os/^{188}Os$ ratios in the earliest Rhaetian (Kuroda et al., 2010; Callegaro et al., 2012; Onoue et al., 2018). Such excursions result from changes in the sedimentary input to the ocean, either through reduction of continental input due to cooling and decreased precipitation, or through increased input from the weathering of mafic igneous sources (Callegaro et al., 2012). Notably, emplacement of a LIP is capable of producing both effects. Acid fallout of H_2SO_4 aerosols, and outgassed chlorides and fluorides could produce abrupt short-term decreases in the pH of surface waters, impacting planktonic autotrophs and the entire marine trophic system (e.g. Hönisch et al., 2012; Greene et al., 2012). Aside from slowing ocean circulation, subsequent warming also can affect the marine realm in the longer term through enhanced chemical weathering that leads to increased delivery of

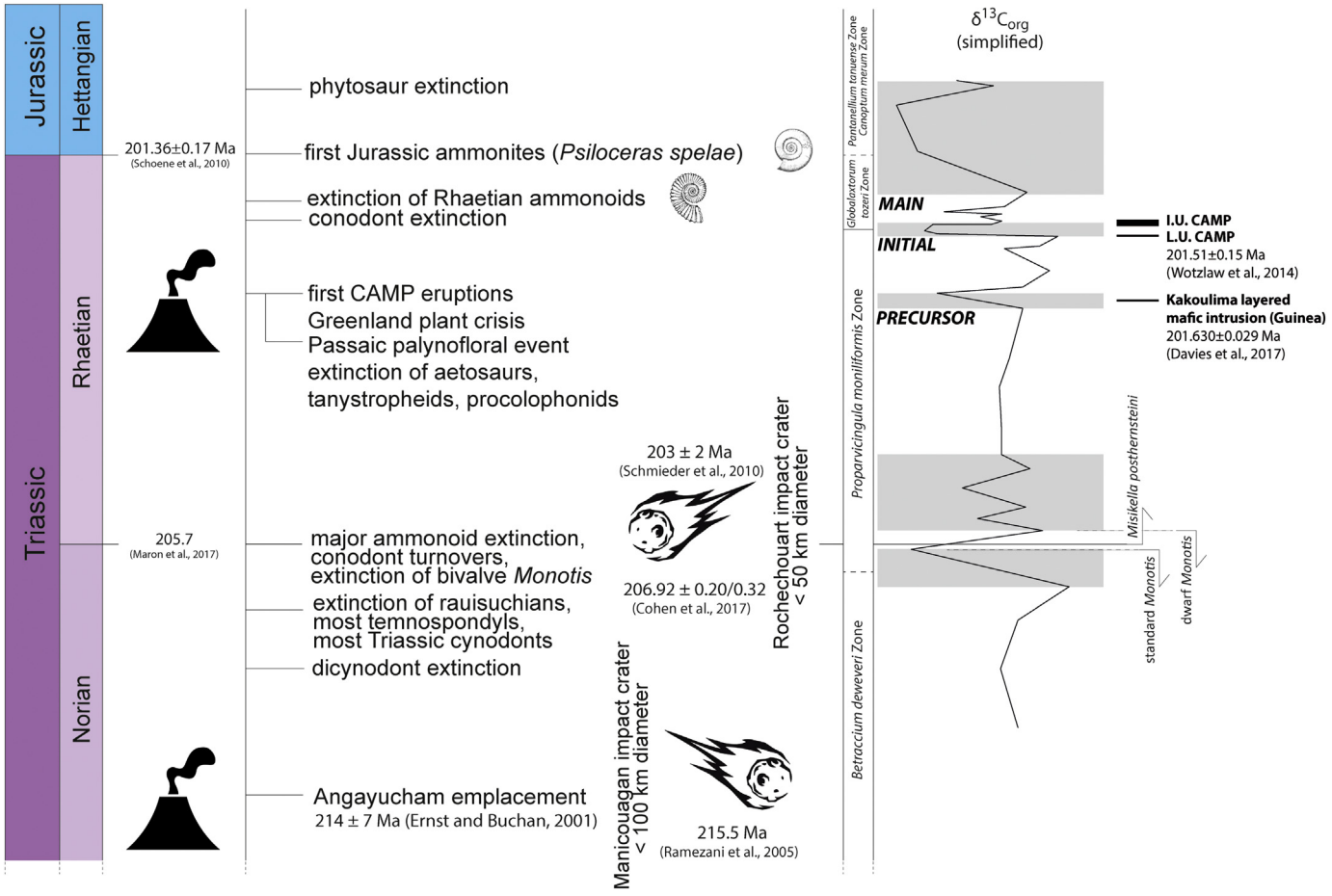

Fig. 5. Schematic diagram of events occurred close to the Norian/Rhaetian boundary (NRB), including faunal and floristic turnovers, impact craters, Large Igneous Provinces (LIPs), and simplified $\delta^{13}C_{org}$ curve of the latest Triassic – earliest Jurassic (not in scale).

nutrients to the ocean, with an increase in %TOC, as is seen in the Lagonegro Basin (Rigo et al., 2016; Zaffani et al., 2017) and in British Columbia (Ward et al., 2001, 2004).

Therefore, a possible trigger for the Norian-Rhaetian conditions could have been vast emissions of greenhouse gases during large-scale volcanic activity, such as the emplacement of a Large Igneous Province (LIP). Two LIPs documented during the latest Triassic–earliest Jurassic are the CAMP (the Central Atlantic Magmatic Province) and the volcanics of the Angayucham Terrane. The CAMP is represented by the subaerial tholeiitic basalts and intrusive bodies (ca. 1.5–3 million km^3), emplaced in the central portion of the supercontinent Pangaea, straddling the palaeoequator (e.g., Marzoli et al., 2018). The NRB has been astronomically intercalibrated (Maron et al., 2015) and radioisotopically dated (Wotzlaw et al., 2014) at 205.7 Ma, while the oldest known radiometrically dated CAMP igneous rocks (Kakoulima layered mafic intrusion, Guinea) yield an age of ca. 201.63 Ma (Davies et al., 2017). Therefore, CAMP is ca. 4 Ma too young to have caused the CIE across the NRB (Fig. 5).

The other known Late Triassic LIP is the Angayucham oceanic plateau and oceanic islands complex accreted onto the Brooks Range (Pallister et al., 1989), cropping out in Alaska, with an estimated age of 214 ± 7 Ma (Ernst and Buchan, 2001; Prokoph et al., 2013). The estimated total volume of the Angayucham LIP, evaluated from the areal extent of ophiolite outcrops, ranges between 225 and 450 × 10^3 km^3 (Ernst and Buchan, 2001; Prokoph et al., 2013). Considering the uncertainty of the age of the Angayucham LIP and the estimated age of ca. 207 Ma for the beginning of both the $\delta^{13}C_{org}$ and the stepwise extinction, the Angayucham LIP seems a potential candidate for triggering the events recorded across the NRB (Fig. 5). It is noteworthy that the exposed Alaskan rocks likely greatly under-represent the original volume of volcanic basalts as a consequence of the obduction of the Angayucham terrane onto the Brooks Range continental margin (Pallister et al., 1989). Moreover, the radiometric age of 214 ± 7 Ma (Ernst and Buchan, 2001; Prokoph et al., 2013) probably represents only a portion of the entire LIP, and younger material is either not preserved or has not yet been radioisotopically calibrated.

The inconsistencies in age estimates for the onset of the Angayucham basalts lead to two possible scenarios for the perturbation of the $\delta^{13}C$ curve around the NRB. In the first scenario, an as-yet undocumented LIP body was emplaced at ca. 207 Ma (post-Angayucham, pre-CAMP), close to the base of the Rhaetian, during the Sevatian (late Norian). The onset of this volcanism played the role of the main trigger for the NRB climatic and geochemical perturbation. This scenario is compatible with the stepwise turnover of major Triassic marine groups such as conodonts, radiolarians, ammonoids, and cosmopolitan bivalves (Tanner et al., 2004; Lucas and Tanner, 2018), starting dramatically around the NRB and culminating just before the TJB (Hallam, 2002; Tanner et al., 2004; Wignall et al., 2007) (Fig. 5). In the second scenario, undocumented late Norian volcanic activity was part of the geodynamic evolution of Pangaea during the Late Triassic-Early Jurassic, which included Central Atlantic rifting previously documented from the late Norian (Cleveland et al., 2008). This scenario does not involve the Angayucham or CAMP basalts, other than the role of the latter in the late Rhaetian ETE, as documented by radioisotopic age determinations (Blackburn et al., 2013).

Lastly, we note that destabilization of clathrates has been cited as a contributing factor toward the negative CIE associated with the ETE (e.g., Pálfy et al., 2001; Van de Schootbrugge et al., 2008), which could

have been triggered variously by volcanic activity or a bolide impact (Fig. 5). Tanner et al. (2004) noted the difficulties associated with this hypothesis, however, not least amongst them the lack of supporting evidence. Moreover, the later part of the Norian stage (Sevatian) is generally considered an interval of overall warm climate based on the $\delta^{18}O$ of conodont apatite (Trotter et al., 2015) and other sedimentary evidence (Tanner, 2018), which calls into question the depth and mass of clathrate available in the deep ocean for dissociation. More significantly, the abrupt positive shift of $\delta^{18}O$ values early in the Rhaetian indicates a cooling episode, contra-indicating the sudden release of methane. At present, we find no evidence to support this mechanism as the driver of the negative CIE at the NRB.

6. Conclusions

In summary, our data document the global extent of a substantial perturbation to the carbon cycle that spanned the NRB. The CIE described herein extended across the Panthalassa Ocean to both sides of the Pangaean supercontinent and is recorded in both the Northern and Southern Hemispheres. The onset of the stepwise Late Triassic extinctions coincided with this NRB carbon perturbation, indicating that the combination of climate and environmental changes impacted the biota at this time. We suggest that the most likely proximal cause of the negative shift in $\delta^{13}C_{org}$ at the NRB was a large-volume emission of greenhouse gases from a large-scale volcanic event pre-dating the NRB. As no LIP dated to this time is yet known, we acknowledge that alternative sources of greenhouse gas emissions, or other mechanisms of carbon-cycle disruption, are possible. Further investigation is needed to better understand the dynamics that induced the disturbance of the carbon cycle during the Late Triassic.

Funding

This study was supported by the grants CPDA152211/15 to Manuel Rigo by the University of Padova and the PRIN 2017W2MARE by the Italian MIUR (Ministero dell'Istruzione, dell'Università e della Ricerca) to Manuel Rigo; and by the Japan Society for the Promotion of Science (grants 16KK0104 and 17H02975 to Tetsuji Onoue). Kliti Grice and Jaime Cesar acknowledge the Australian Research Council for Linkage funding (LP150100341). Lydia Tackett would like to acknowledge funding from her NSF CAREER grant 1654088. Hamish Campbell was supported by GNS Science Zealandia Programme with funding from MBIE (Ministry for Business, Innovation and Employment; New Zealand Government).

Author contributions

MR developed the theory and conceived the study, and with MZ, MEK and LG analysed the organic matter, interpreted the data and wrote the manuscript. TO, FT, DY analysed and interpreted the geochemical data and contributed to writing the manuscript. KG and JC acquisition of data, analysis of data, interpretation and contribution to writing of manuscript on the northwest shelf. LT and SL contributed with the biotic turnover analyses and improved the manuscript. MM provided the age model and comments on the manuscript. CA, GC, LST, HC, MZ, AB provided advice and comments on the manuscript. Field work by MR, MM, TO, LST, HC, MZ, MC, AB.

Declaration of Competing Interests

Authors declare no competing interests;

Data and materials availability

All data available in the main text or the supplementary materials.

Acknowledgments

This research used samples provided by the Ocean Discovery Program (ODP, Site 761C) assisted by Dr. L. Gupta (IODP Curator, Kochi Core Center - KCC), who is warmly thanked. We are grateful for the constructive reviews of this study provided by two anonymous Reviewers and by the Editor A. Negri.

Appendix A. Supplementary data

Supplementary data to this article can be found online at https://doi.org/10.1016/j.earscirev.2020.103180.

References

Abdala, F., Gaetano, L.C., 2018. Late Triassic cynodont life: time of innovations in the mammal lineage. In: Tanner, L.H. (Ed.), The Late Triassic world: earth in a time of transition. Topics in Geobiology 11. Springer, pp. 407–445.
Aldridge, F., Smith, M.P., 1993. Conodonta. In: Benton, M.J. (Ed.), The Fossil Record 2. Chapman and Hall, London, pp. 563–572.
Allasinaz, A., 1992. The Late Triassic-Hettangian bivalve turnover in Lombardy (Southern Alps). Riv. Ital. Paleot. Strat. 53, 1211–1235.
Amodeo, F., 1999. Il Triassico terminale–Giurassico del Bacino Lagonegrese: Studi stratigrafici sugli Scisti Silicei della Basilicata (Italia meridionale). Lausanne, Mem. Geol. 33, 1–123.
Barbacka, M., Pacyna, G., Kocsis, Á.T., Jarzynka, A., Ziaja, J., Bodor, E., 2017. Changes in terrestrial floras at the Triassic-Jurassic Boundary in Europe. Palaeogeogr. Palaeoclimatol. Palaeoecol. 480, 80–93.
Bartolini, A., Guex, J., Spangenberg, J.E., Schoene, B., Taylor, D.G., Schaltegger, U., Atudorei, V., 2012. Disentangling the Hettangian carbon isotope record: Implications for the aftermath of the end-Triassic mass extinction. Geochem. Geophys. Geosyst. 13, Q01007. https://doi.org/10.1029/2011GC003807.
Bazzucchi, P., Bertinelli, A., Ciarapica, G., Marcucci, M., Passeri, L., Rigo, M., Roghi, G., 2005. The Late Triassic–Jurassic stratigraphic succession of Pignola (Lagonegro-Molise Basin, Southern Apennines, Italy). Boll. Soc. Geol. It. 124, 143–153.
Benton, M.J., Twitchett, R.J., 2003. How to kill (almost) all life: The end-Permian extinction event. Trends Ecol. Evol. 18, 358–365.
Bertinelli, A., Ciarapica, G., De Zanche, V., Marcucci, M., Mietto, P., Passeri, L., Rigo, M., Roghi, G., 2005. Stratigraphic evolution of the Triassic–Jurassic Sasso di Castalda succession (Lagonegro basin, Southern Apennines, Italy). Boll. Soc. Geol. It. 124, 177–188.
Bertinelli, A., Casacci, M., Concheri, G., Gattolin, G., Godfrey, L., Katz, M.E., Maron, M., Mazza, M., Mietto, P., Muttoni, G., Rigo, M., Sprovieri, M., Stellin, F., Zaffani, M., 2016. The Norian/ Rhaetian boundary interval at Pignola-Abriola section (southern Apennines, Italy) as a GSSP candidate for the Rhaetian stage: An update. Albertiana 43, 6–19.
Blackburn, T.J., Olsen, P.E., Bowring, S.A., McLean, N.M., Kent, D.V., Puffer, J., McHone, G., Rasbury, T., Et-Touhami, M., 2013. Zircon U-Pb geochronology links the End-Triassic extinction with the Central Atlantic Magmatic Province. Science 340, 941–945.
Bonis, N.R., Kürschner, W.M., Krystyn, L., 2009. A detailed palynological study of the Triassic–Jurassic transition in key sections of the Eiberg Basin (Northern Calcareous Alps, Austria). Rev. Palaeobot. Palynol. 156, 376–400.
Bralower, T.J., Bown, P.R., Siesser, W.G., 1992. Upper Triassic calcareous nannoplankton biostratigraphy, Wombat Plateau, northwest Australia. Proc. Ocean Drill. Program Sci. Results 122, 437–451.
Brenner, W., Bown, P.R., Bralower, T.J., Crasquin-Soleau, S., Depeche, F., Dumont, T., Martini, R., Siesser, W.G., Zaninetti, L., 1992. Correlation of Carnian to Rhaetian palynological, foraminiferal, calcareous nannofossil, and ostracode biostratigraphy, Wombat Plateau. Proc. Ocean Drill. Program Sci. Results 122, 487–495.
Brunn, J.H., 1956. Contribution à l'étude géologique du Pinde septentrional et d'une partie de la Macédonie occidentale. Ann. Géol. Pays Helléniques 7, 1–358.
Callegaro, S., Rigo, M., Chiaradia, M., Marzoli, A., 2012. Latest Triassic marine Sr isotopic variations, possible causes and implications. Terra Nova 24, 130–135.
Cameron, B.E.B., Tipper, H.W., 1985. Jurassic stratigraphy of the Queen Charlotte Islands, British Columbia. GSA Bull. 365, 49.
Carter, E.S., 1993. Biochronology and Paleontology of uppermost Triassic (Rhaetian) radiolarians, Queen Charlotte Islands, British Columbia, Canada. Lausanne, Switzerland, Mem. Geol. 11, 1–176.
Carter, E.S., 1994. Evolutionary trends in the latest Norian through Hettangian radiolarians from the Queen Charlotte Islands, British Columbia. Geob. Mém. Spéc. 17, 111–119.
Carter, E.S., Hori, R.S., 2005. Global correlation of the radiolarian faunal change across the Triassic Jurassic boundary. Can. J. Earth Sci. 42 (5), 777–790.
Casacci, M., Bertinelli, A., Algeo, T.J., Rigo, M., 2016. Carbonate to biosilica transition at the Norian-Rhaetian boundary controlled by rift-related subsidence in the western Tethyan Lagonegro Basin (southern Italy). Palaeogeogr. Palaeoclimatol. Palaeoecol. 456, 21–36.
Cesar, J., Grice, K., 2017. $\delta^{13}C$ of polycyclic aromatic hydrocarbons to establish the facies variations in a fluvial deltaic Triassic record (Dampier sub-Basin, Western Australia). Org. Geochem. 107, 59–68.

Cesar, J., Grice, K., 2019. Molecular fingerprint from plant biomarkers in Triassic-Jurassic petroleum source rocks from the Dampier sub-Basin, Northwest Shelf of Australia. Mar. Petrol. Geol. 110, 189–197.
Ciarapica, G., Passeri, L., 1998. Evoluzione paleogeografica degli Appennini: Atti Tic. Sc. Terra 40, 233–290.
Clapham, M.E., Karr, J.A., 2012. Environmental and biotic controls on the evolutionary history of insect body size. PNAS 109, 10927–10930.
Clapham, M.E., Renne, P.R., 2018. Flood basalts and mass extinctions. Annu. Rev. Earth Planet. 47, 275–303. https://doi.org/10.1146/annurev-earth-053018- 060136.
Clark, D.L., 1980. Rise and fall of Triassic conodonts. Am. Assoc. Petrol. Geol. Bull. 64, 691.
Clark, D.L., 1981. Extinction of Triassic conodonts. Geol. Bundesanst. Abhand. 35, 193–195.
Clark, D.L., 1983. Extinction of conodonts. J. Paleontol. 57, 652–661.
Cleveland, D.M., Nordt, L.C., Dworkin, S.I., Atchley, S.C., 2008. Pedogenic carbonate isotopes as evidence for extreme climatic events preceding the Triassic-Jurassic boundary: Implications for the biotic crisis? Geol. Soc. Am. Bull. 120, 1408–1415.
Clutson, M.J., Brown, D.E., Tanner, L.H., 2018. Distal processes and effects of multiple Late Triassic terrestrial bolide impacts: Insights from the Norian Manicouagan event, northeastern Quebec, Canada. In: Tanner, L.H. (Ed.), The Late Triassic World: Earth in a Time of Transition. Topics in Geobiology 46. Springer, pp. 127–187.
Cohen, B.E., Mark, D.F., Lee, M.R., Simpson, S.L., 2017. A new high-precision $^{40}Ar/^{39}Ar$ age for the Rochechouart impact structure: At least 5 Ma older than the Triassic–Jurassic boundary. Meteorit. Planet. Sci. 52, 1600–1611.
Condamine, F.L., Clapham, M.E., Kergoat, G.J., 2016. Global patterns of insect diversification: Towards a reconciliation of fossil and molecular evidence? Scient. Rep. 6, 19208.
Coplen, T.B., Brand, W.A., Gehre, M., Groning, M., Meijer, H.A.J., Toman, B., Verkouteren, R.M., 2006. New guidelines for $\delta^{13}C$ measures. Anal. Chem. 78, 2439–2441.
Dagys, A.S., Dagys, A.A., 1994. Global correlation of the terminal Triassic. In: Guex, J., Baud, A. (Eds.), Recent Developments on Triassic Stratigraphy. Memoires de Geologie, Lausanne 22. pp. 25–34.
Dal Corso, J., Marzoli, A., Tateo, F., Jenkyns, H.C., Bertrand, H., Youbi, N., Mahmoudi, A., Font, E., Buratti, N., Cirilli, S., 2014. The dawn of CAMP volcanism and its bearing on the end-Triassic carbon cycle disruption. J. Geol. Soc. Lond. 171, 153–164. https://doi.org/10.1144/jgs2013-063.
Dal Corso, J., Gianolla, P., Rigo, M., Franceschi, M., Roghi, G., Mietto, P., Manfrin, S., Raucsik, B., Budai, T., Jenkyns, H., Reymond, C., Caggiati, M., Gattolin, G., Breda, A., Merico, A., Preto, N., 2018. Multiple negative carbon-isotope excursions during the Carnian Pluvial Episode (Late Triassic). Earth-Sci. Rev. 185, 732–750. https://doi.org/10.1016/j.earscirev.2018.07.004.
Davies, J.H.F.L., Marzoli, A., Bertrand, H., Youbi, N., Ernesto, M., Schaltegger, U., 2017. End-Triassic mass extinction started by intrusive CAMP activity. Nat. Commun. 8, 15596.
De Renzi, M., Budurov, K., Sudar, M., 1996. The extinction of conodonts in terms of discrete elements at the Triassic-Jurassic boundary. Cuader Geolog Ibèrica 20, 347–364.
Deenen, M.H.L., Ruhl, M., Bonis, N.R., Krijgsman, W., Kuerschner, W.M., Reitsma, M., van Bergen, M.J., 2010. A new chronology for the end-Triassic mass extinction. Earth Planet. Sci. Lett. 291, 113–125.
Degnan, P.J., Robertson, A.H.F., 1998. Mesozoic–early Tertiary passive margin evolution of the Pindos Ocean (NW Peloponnese, Greece). Sediment. Geol. 117, 33–70.
D'hondt, S., Donaghay, P., Zachos, J.C., Luttenberg, D., Lindinger, M., 1998. Organic carbon fluxes and ecological recovery from the Cretaceous-Tertiary mass extinction. Science 282, 276–279.
Diakow, L., Orchard, M.J., Friedman, R., 2011. Absolute ages for the Norian Stage: A contribution from southern British Columbia, Canada. Can. Paleontol. Conf. Proc. 9, 27–28.
Diakow, L., Orchard, M.J., Friedman, R., 2012. Absolute ages for the Norian Stage: A further contribution from southern British Columbia, Canada. In: Cordilleran Tectonics Workshop: Geological Association Canada, Pacific Section, Program and Abstracts, pp. 2.
Du, Y., Chiari, M., Karádi, V., Nicora, V., Onoue, T., Pálfy, J., Roghi, G., Tomimatsu, Y., Rigo, M., 2020. The asynchronous disappearance of conodonts: new constraints from Triassic – Jurassic boundary sections in the Tethys and Panthalassa. Earth-Sci. Rev. https://doi.org/10.1016/j.earscirev.2020.103176.
Ernst, R.E., Buchan, K.L., 2001. Large mafic magmatic events through time and links to mantle-plume heads. Geol. Soc. Am. Spec. Pap. 352, 483–575.
Erwin, D.H., 2006. Extinction: How Life on Earth Nearly Ended 250 Million Years Ago. Princeton University Press, Princeton, New Jersey.
Exon, N.F., von Rad, U., 1994. The Mesozoic and Cainozoic sequences of the Northwest Australian Margin, as revealed by ODP Core Drilling and related studies. In: Purcell, P.G., Purcell, P.R. (Eds.), The Sedimentary Basins of Western Australia. Proceedings of the Western Australian Basins Symposium, Perthpp. 181–200.
Fio, K., Spangenberg, J.E., Vlahovic, I., Sremac, J., Velic, I., Mrinjek, E., 2010. Stable isotope and trace element stratigraphy across the Permian-Triassic transition: A redefinition of the boundary in the Velebit Mountain, Croatia. Chem. Geol. 278, 38–57. https://doi.org/10.1016/j.chemgeo.2010.09.001.
Flügel, E., 2002. Triassic reef patterns. In: Kiessling, W., Fluegel, E., Golonka, J. (Eds.), Phanerozoic Reef Patterns. SEPM Spec. Publ. 72. pp. 391–463.
Flügel, E., Kiessling, W., 2002. Patterns of Phanerozoic reef crises. In: Kiessling, W., Fluegel, E., Golonka, J. (Eds.), Phanerozoic Reef Patterns. SEPM Spec. Publ. 72. pp. 691–734.
Flügel, E., Senowbari-Daryan, B., 2001. Triassic reefs of the Tethys. In: Stanley Jr.G.D. (Ed.), The history and sedimentology of ancient reef systems. Kluwer Academic/Plenum Publishers, New York, pp. 217–249.
Furin, S., Preto, N., Rigo, M., Roghi, G., Gianolla, P., Crowley, J.L., Bowring, S.A., 2006. High precision U-Pb zircon age from the Triassic of Italy: Implications for the Triassic time scale and the Carnian origin of calcareous nannoplankton and dinosaurs. Geology 34, 1009–1012. https://doi.org/10.1130/G22967A.1.
Galli, M.T., Jadoul, F., Bernasconi, S.M., Weissert, H., 2005. Anomalies in global carbon cycling at the Triassic/Jurassic boundary: Evidence from a marine C-isotope record. Palaeogeogr. Palaeoclimatol. Palaeoecol. 216, 203–214. https://doi.org/10.1016/j.palaeo.2004.11.009.
Galli, M.T., Jadoul, F., Bernasconi, S.M., Cirilli, S., Weissert, H., 2007. Stratigraphy and palaeoenvironmental analysis of the Triassic–Jurassic transition in the western Southern Alps (Northern Italy). Palaeogeogr. Palaeoclimatol. Palaeoecol. 244, 52–70. https://doi.org/10.1016/j.palaeo.2006.06.023.
Gardin, S., Krystyn, L., Richoz, S., Bartolini, A., Galbrun, B., 2012. Where and when the earliest coccolithophores? Lethaia 45, 507–523.
Giordano, N., Rigo, M., Ciarapica, G., Bertinelli, A., 2010. New biostratigraphical constraints for the Norian/Rhaetian boundary: Data from Lagonegro Basin, Southern Apennines, Italy. Lethaia 43, 573–586. https://doi.org/10.1111/j.1502-3931.2010.00219.x.
Giordano, N., Ciarapica, G., Bertinelli, A., Rigo, M., 2011. The Norian–Rhaetian interval in two sections of the Lagonegro area. The transition from carbonate to siliceous deposition. Ital. J. Geosci. 130, 380–393.
Grant-Mackie, J.A., 1981. New Zealand Warepan (Upper Triassic) sequences: Murihiku Supergroup of the North Island. J. R. Soc. New Zeal. 11, 31–56.
Grant-Mackie, J.A., 2013. *Makoiamya cotterallae*, a new genus and species of bivalve (Ceratomyidae) from the latest Triassic of New Zealand and New Caledonia. Zootaxa 3741, 327–348.
Greene, S.E., Martindale, R.C., Ritterbush, K.A., Bottjer, D.J., Corsetti, F.A., Berelson, W.M., 2012. Recognising ocean acidification in deep time: An evaluation of the evidence for acidification across the Triassic-Jurassic boundary. Earth-Sci. Rev. 113 (1-2), 72–93.
Grice, K., Backhouse, J., Alexander, R., Marshall, N., Logan, G.A., 2005. Correlating terrestrial signatures from biomarker distributions, $\delta^{13}C$, and palynology in fluvio-deltaic deposits from NW Australia (Triassic–Jurassic). Org. Geochem. 36, 1347–1358.
Grice, K., Nabbefeld, B., Maslen, E., 2007. Source and significance of selected polycyclic aromatic hydrocarbons in sediments (Hovea-3 well, Perth Basin, Western Australia) spanning the Permian-Triassic boundary. Org. Geochem. 38, 1795–1803.
Grimaldi, D., Engel, M.S., 2005. Evolution of the Insects. Cambridge University Press, Cambridge, pp. 1–755.
Guex, J., 2016. Retrograde evolution during major extinction crises. Springer, Heidelberg.
Guex, J., Bartolini, A., Taylor, D., 2002. Discovery of *Neophyllites* (Ammonita, Cephalopdda, early Hettangian) in the New York Canyon sections (Gabbs Valley Range, Nevada) and discussion of the $\delta^{13}C$ negative anomalies located around the Triassic-Jurassic boundary. Bull. Soc. Vaud. Sci. Natur. 88, 247–255.
Guex, J., Bartolini, A., Atudorei, Taylor D., 2003. Two negative $\delta^{13}C_{org}$ excursions near the Triassic-Jurassic boundary in the New York Canyon area (Gabbs Valley Range, Nevada). Bull. Géol. Lausanne 360, 1–4.
Guex, J., Bartolini, A., Atudorei, V., Taylor, D., 2004. High resolution ammonite and carbon isotope stratigraphy across the Triassic–Jurassic boundary at New York Canyon (Nevada). Earth Planet. Sci. Lett. 225, 29–41.
Hallam, A., 2002. How catastrophic was the end-Triassic mass extinction? Lethaia 35, 147–157.
Hallam, A., Wignall, P.B., 1997. Mass Extinctions and Their Aftermath. Oxford University Press, Oxford.
Hayes, J.M., Strauss, H., Kaufman, A.J., 1999. The abundance of ^{13}C in marine organic matter and isotopic fractionation in the global biogeochemical cycle of carbon during the past 800 Ma. Chem. Geol. 161, 103–125. https://doi.org/10.1016/S0009-2541(99)00083-2.
Hesselbo, S.P., Robinson, S.A., Surlyk, F., Piasecki, S., 2002. Terrestrial and marine extinction at the Triassic-Jurassic boundary synchronized with major carbon-cycle perturbation: A link to initiation of massive volcanism? Geology 30, 251–254.
Hesselbo, S.P., McRoberts, C.A., Pálfy, J., 2007. Triassic-Jurassic boundary events: Problems, progress, possibilities. Palaeogeogr. Palaeoclimatol. Palaeoecol. 244, 1–4.
Hocking, R.M., Moors, H.T., Van de Graaff, W.J.E., 1987. Geology of the Carnarvon Basin, Western Australia. Geological Survey of Western Australia, Perth.
Hodych, J.P., Dunning, F.R., 1992. Did the Manicouagan impact trigger end-of-Triassic mass extinction? Geology 20, 51–54.
Hönisch, B., Ridgwell, A., Schmidt, D.N., Thomas, E., Gibbs, S.J., Sluijs, A., Zeebe, R., Kump, L., Martindale, R.C., Greene, S.E., Kiessling, W., Ries, J., Zachos, J.C., Royer, D.L., Barker, S., Marchitto Jr., T.M., Moyer, R., Pelejero, C., Ziveri, P., Foster, G.L., Williams, B., 2012. The geological record of ocean acidification. Science 335 (6072), 1058–1063.
House, M.R., 1963. Burst in evolution. Adv. Sci. 19, 499–507.
Jenkyns, H.C., 2010. Geochemistry of oceanic anoxic events. Geochem. Geophys. Geosyst. 11, Q03004.
Jiang, C., Alexander, R., Kagi, R.I., Murray, A.P., 1998. Polycyclic aromatic hydrocarbons in ancient sediments and their relationships to palaeoclimate. Org. Geochem. 29, 1721–1735.
Jiang, L., Planavsky, N., Zhao, M., Liu, W., Wang, X., 2019. Authigenic origin for a massive negative carbon isotope excursion. Geology 47, 115–118. https://doi.org/10.1130/G45709.1.
Jones, C.E., Jenkyns, H.C., 2001. Seawater strontium isotopes, oceanic anoxic events, and seafloor hydrothermal activity in the Jurassic and Cretaceous. Am. J. Sci. 301, 112–149.
Kafousia, N., Karakitsios, V., Jenkyns, H.C., Mattioli, E., 2011. A global event with a

regional character: The Early Toarcian Oceanic Anoxic Event in the Pindos Ocean (northern Peloponnese, Greece). Geol. Mag. 148, 619–631.
Karádi, V., Cau, A., Mazza, M., Rigo, M., 2019. The last phase of conodont evolution during the Late Triassic: Integrating biostratigraphic and phylogenetic approaches. Palaeogeogr. Palaeoclimatol. Palaeoecol. https://doi.org/10.1016/j.palaeo.2019.03.045.
Karr, J.A., Clapham, M.E., 2015. Taphonomic biases in the insect fossil record: Shifts in articulation over geologic time. Paleobiology 41, 16–32.
Kennedy, W.J., 1977. Ammonite evolution. Dev. Palaeontol. Stratigr. 5, 251–304. https://doi.org/10.1016/S0920-5446(08)70328-5.
Kent, D.V., Cramer, B.S., Lanci, L., Wang, D., Wright, J.D., Van der Voo, R., 2003. A case for a comet impact trigger for the Paleocene/Eocene thermal maximum and carbon isotope excursion. Earth Planet. Sci. Lett. 211, 13–26. https://doi.org/10.1016/S0012-821X(03)00188-2.
Kent, D.V., Olsen, P.E., Muttoni, G., 2017. Astrochronostratigraphic polarity time scale (APTS) for the Late Triassic and Early Jurassic from continental sediments and correlation with standard marine stages. Earth Sci. Rev. 166, 153–180.
Kiessling, W., 2001. Paleoclimatic significance of Phanerozoic reefs. Geology 29, 751–754.
Kiessling, W., Danelian, T., 2011. Trajectories of late Permian - Jurassic radiolarian extinction rates: No evidence for an end-Triassic mass extinction. Fossil Record 14, 95–101.
Kiessling, W., Fluegel, E., Golonka, J., 1999. Paleoreef maps: Evaluation of a comprehensive database on Phanerozoic reefs. Am. Assoc. Petrol. Geol. Bull. 83, 1552–1587.
Kiessling, W., Aberhan, M., Brenneis, B., Wagner, P., 2007. Extinction trajectories of benthic organisms across the Triassic-Jurassic boundary. Palaeogeogr. Palaeoclimatol. Palaeoecol. 244 (1–4), 201–222. https://doi.org/10.1016/j.palaeo.2006.06.029.
Knobbe, T.K., Schaller, M.F., 2018. A tight coupling between atmospheric pCO_2 and sea-surface temperature in the Late Triassic. Geology 46, 43–46.
Korte, C., Kozur, H.W., Bruckschen, P., Veizer, J., 2003. Strontium isotope evolution of Late Permian and Triassic seawater. Geochim. Cosmochim. Acta 67, 47–62.
Korte, C., Kozur, H.W., Veizer, J., 2005. ^{13}C and ^{18}O values of Triassic brachiopods and carbonate rocks as proxies for coeval seawater and palaeotemperature. Palaeogeogr. Palaeoclimatol. Palaeoecol. 226, 287–306. https://doi.org/10.1016/j.palaeo.2005.05.018.
Kozur, H., Mock, R., 1991. New Middle Carnian and Rhaetian conodonts from Hungary and the Alps, stratigraphic importance and tectonic implications for the Buda Mountains and adjacent areas. J. Geol. Bundesanst. 134, 271–297.
Kozur, H.W., Weems, R.E., 2010. The biostratigraphic importance of conchostracans in the continental Triassic of the northern hemisphere. In: Lucas, S.G. (Ed.), The Triassic timescale. Geol. Soc. London Spec. Publ. 334. pp. 315–417.
Krystyn, L., 2010. Decision report on the defining event for the base of the Rhaetian stage. Albertiana 38, 11–12.
Krystyn, L., Bouquerel, H., Kueschner, W., Richoz, S., Gallet, Y., 2007. Proposal for a candidate GSSP for the base of the Rhaetian Stage. New Mex. Mus. Nat. Hist. Sci. Bull. 41, 189–199.
Kummel, B., 1957. Triassic Ammonoidea. In: Arkell, W.J., Furnish, W.M., Kummel, B., Miller, A.K., Moore, R.C., Schindewolf, O., Sylvester-Bradley, P.C., Wright, C.W. (Eds.), Treatise on inverterbrate paleontology, Part L, Mollusca 4. Geological Society of America and University of Kansas Press, Cephalopoda.
Kuroda, J., Hori, R.S., Suzuki, K., Grocke, D.R., Ohkouchi, N., 2010. Marine osmium isotope record across the Triassic-Jurassic boundary from a Pacific pelagic site. Geology 38, 1095–1098.
Kürschner, W.M., Bonis, N.R., Krystyn, L., 2007. Carbon-isotope stratigraphy and palynostratigraphy of the Triassic-Jurassic transition in the Tiefengraben section - Northern Calcareous Alps (Austria). Palaeogeogr. Palaeoclimatol. Palaeoecol. 244 (1–4), 257–280.
Kustatscher, E., Ash, S.R., Karasev, E., Ptt, C., Vajda, V., Yu, J., McLoughlin, S., 2018. The Late Triassic flora. In: Tanner, L.H. (Ed.), The Late Triassic world: Earth in a time of transition. Topics in Geobiology 13. Springer, pp. 545–622.
Labandeira, C.C., 2005. The fossil record of insect extinction: New approaches and future directions. Am. Entomol. Spring 2005, 310–315.
Labandeira, C.C., Sepkoski Jr., J.J., 1993. Insect diversity in the fossil record. Science 261, 310–315.
Lambert, P., 2010. Target and impact deposits at Rochechouart impact structure, France. Geol. Soc. Am. Spec. Pap. 465, 509–541.
Laws, R.A., 1982. Late Triassic depositional environments and molluscan associations from west-central Nevada. Palaeogeogr. Palaeoclimatol. Palaeoecol. 37, 131–148.
Longley, I., Buessenschuett, C., Clydsdale, L., Cubitt, C., Davis, R., Johnson, M., Marshall, N., Murray, A., Somerville, R., Spry, T., Thompson, N., 2002. The North West Shelf of Australia – a Woodside Perspective. In: Keep, M., Moss, S. (Eds.), The Sedimentary Basins of Western Australia 3: Proceedings of the Petroleum Exploration Society of Australia Symposium. Petroleum Exploration Society of Australia, pp. 27–88.
Longridge, L.M., Carter, E.S., Smith, P.L., Tipper, H.W., 2007. Early Hettangian ammonites and radiolarians from the Queen Charlotte Islands, British Columbia and their bearing on the definition of the Triassic-Jurassic boundary. Palaeogeogr. Palaeoclimatol. Palaeoecol. 244, 142–169.
Lucas, S.G., 2010. The Triassic timescale based on nonmarine tetrapod biostratigraphy and biochronology. In: Lucas, S.G. (Ed.), The Triassic timescale. Geol. Soc. London. Spec. Publ. 334. pp. 447–500.
Lucas, S.G., 2018a. Late Triassic Ammonoids: Distribution, Biostratigraphy and Biotic Events. In: Tanner, L.H. (Ed.), The Late Triassic world: Earth in a time of transition. Topics in Geobiology 7. Springer, pp. 237–261.
Lucas, S.G., 2018b. Late Triassic terrestrial tetrapods: Biostratigraphy, biochronology and biotic events. In: Tanner, L.H. (Ed.), The Late Triassic world: Earth in a time of transition. Topics in Geobiology 10. Springer, pp. 351–405.
Lucas, S.G., Heckert, A.B., 2011. Late Triassic aetosaurs as the trackmaker of the terapod footprint ichnotaxon *Brachychirotherium*. Ichnos 18, 197–208.
Lucas, S.G., Tanner, L.H., 2007. The nonmarine Triassic-Jurassic boundary in the Newark Supergroup of eastern North America. Earth-Sci. Rev. 84, 1–20.
Lucas, S.G., Tanner, L.H., 2008. Reexamination of the end-Triassic mass extinction. In: Elewa, A.M.T. (Ed.), Mass extinction. Springer Verlag, New York, pp. 66–103.
Lucas, S.G., Tanner, L.H., 2015. End-Triassic nonmarine biotic events. J. Paleogeogr. 4, 331–348.
Lucas, S.G., Tanner, L.H., 2018. The missing mass extinction at the Triassic-Jurassic boundary. In: Tanner, L.H. (Ed.), The Late Triassic World. Topics in Geobiology 46 Springer, Cham, pp. 721–785.
Lucas, S.G., Hunt, A.P., Hecker, A.B., Spielmann, J.A., 2007. Global Triassic tetrapod biostratigraphy and biochronology: 2007 status. New Mex. Mus. Nat. Hist. Sci. Bull. 41, 229–240.
Lucas, S.G., Tanner, L.H., Kozur, H.W., Weems, R.E., Heckert, A.B., 2012. The Late Triassic timescale: Age and correlation of the Carnian-Norian boundary. Earth-Sci. Rev. 114, 1–8.
Maisch, M.W., Kapitzke, M., 2010. A presumably marine phytosaur (Reptilia: Archisauria) from the pre-planorbis beds (Hettangian) of England. Neues Jahrb. Geol. Paläont. Abhand. 257, 373–379.
Maron, M., Rigo, M., Bertinelli, A., Katz, M.E., Godfrey, L., Zaffani, M., Muttoni, G., 2015. Magnetostratigraphy, biostratigraphy and chemostratigraphy of the Pignola-Abriola section: New constraints for the Norian-Rhaetian boundary. Geol. Soc. Am. Bull. 127, 962–974.
Maron, M., Muttoni, G., Rigo, M., Gianolla, P., Kent, D.V., 2019. New magnetobiostratigraphic results from the Ladinian of the Dolomites and implications for the Triassic geomagnetic polarity timescale. Palaeogeogr. Palaeoclimatol. Palaeoecol. 517, 52–73.
Marshall, N., Lang, S.C., 2013. The sedimentary basins of Western Australia IV. In: Keep, M., Moss, S.J. (Eds.), Proceedings of the Petroleum Exploration Society of Australia Symposium. Petroleum Exploration Society of Australia, pp. 1–32.
Marzoli, A., Bertrand, H., Knight, K.B., Cirilli, S., Buratti, N., Vérati, C., Nomade, S., Renne, P.R., Youbi, N., Martini, R., Allenbach, K., Neuwerth, R., Rapaille, C., Zaninetti, L., Bellieni, G., 2004. Synchrony of the Central Atlantic magmatic province and the Triassic-Jurassic boundary climatic and biotic crisis. Geology 32, 973–976.
Marzoli, A., Callegaro, S., Dal, Corso J., Davies, J.H.F.L., Chiaradia, M., Youbi, N., Bertrand, H., Reisberg, L., Merle, R., Jourdan, F., 2018. The Central Atlantic Magmatic Province (CAMP): A Review. In: Tanner, L.H. (Ed.), The Late Triassic World. Topics in Geobiology 46 Springer, Cham, pp. 91–125.
Maslen, E., Grice, K., Métayer, P.L., Dawson, D., Edwards, D., 2011. Stable carbon isotopic compositions of individual aromatic hydrocarbons as source and age indicators in oils from western Australian basins. Org. Geochem. 42, 387–398.
Mazza, M., Furin, S., Spötl, C., Rigo, M., 2010. Generic turnovers of Carnian/Norian conodonts: Climatic control or competition? Palaeogeogr. Palaeoclimatol. Palaeoecol. 290, 120–137. https://doi.org/10.1016/j.palaeo.2009.07.006.
McElwain, J.C., Beerling, D.J., Woodward, F.I., 1999. Fossil plants and global warming at the Triassic-Jurassic boundary. Science 285, 1386–1390.
McElwain, J.C., Wagner, P.J., Hesselbo, S.P., 2009. Fossil plant relative abundances indicate sudden loss of Late Triassic biodiversity in East Greenland. Science 324, 1554–1556.
McRoberts, C.A., 1994. The Triassic-Jurassic ecostratigraphic transition in the Lombardian Alps, Italy. Palaeogeogr. Palaeoclimatol. Palaeoecol. 110, 145–166.
McRoberts, C.A., 2007. Diversity dynamics and evolutionary ecology of the Middle and Late Triassic halobiid and monotid bivalves. New Mex. Mus. Nat. Hist. Sci. Bull. 41, 272.
McRoberts, C.A., 2010. Biochronology of Triassic bivalves. Geol. Soc. London Spec. Publ. 334, 201–219.
McRoberts, C.A., Newton, C.R., 1995. Selective extinction among end-Triassic European bivalves. Geology 23, 102–104.
McRoberts, C.A., Newton, C.R., Allasinaz, A., 1995. End-Triassic bivalve extinction: Lomabardian Alps. Hist. Biol. 9, 297–317.
McRoberts, C.A., Krystyn, L., Shea, A., 2008. Rhaetian (Late Triassic) *Monotis* (Bivalvia: Pectinoida) from the eastern Northern Calcareous Alps (Austria) and the end-Norian crisis in pelagic faunas. Palaeontology 51, 721–735.
Meyers, P.A., 2014. Why are the $\delta^{13}C_{org}$ values in Phanerozoic black shales more negative than in modern marine organic matter? Geochem. Geophys. Geosyst. 15, 3085–3106.
Mostler, H., Scheuring, B., Urlichs, M., 1978. Zur Mega-, Mikrofauna und Mikroflora der Koessener Schichten (alpine Obertrias) vom Weissloferbach in Tirol unter besonderer Beru€cksichtigung der in der suessi- und marshi- Zone auftretenden Conodonten. Schrift. Erdwiss. Schriftenreihe der Erdwissenschaftlichen Kommissionen 4, 141–174.
Muttoni, G., Kent, D.V., Olsen, P., Di Stefano, P., Lowrie, W., Bernasconi, S., Martin Hernandez, F., 2004. Tethyan magnetostratigraphy from Pizzo Mondello (Sicily) and correlation to the Late Triassic astrochronological polarity time scale. Geol. Soc. Am. Bull. 116, 1043–1058. https://doi.org/10.1130/B25326.1.
Muttoni, G., Kent, D.V., Jadoul, F., Olsen, P.E., Rigo, M., Galli, M.T., Nicora, A., 2010. Rhaetian magneto-biostratigraphy from the Southern Alps (Italy): Constraints on Triassic chronology. Palaeogeogr. Palaeoclimatol. Palaeoecol. 285 (1–2), 1–16.
Muttoni, G., Mazza, M., Mosher, D., Katz, M.E., Kent, D.V., Balini, M., 2014. A Middle–Late Triassic (Ladinian–Rhaetian) carbon and oxygen isotope record from the Tethyan Ocean. Palaeogeogr. Palaeoclimatol. Palaeoecol. 399, 246–259.
Newell, N.D., 1967. Paraconformities. In: Teichert, C., Yochelson, E. (Eds.), Essays in paleontology and stratigraphy. R.C. Moore commemorative volume University of Kansas Press, Lawrence, Kansas, pp. 349–367.
O'Dogherty, L., Carter, E.S., Gorican, S., Dumitrica, P., 2010. Triassic radiolarian biostratigraphy. In: Lucas, S.G. (Ed.), The Triassic timescale. Geol. Soc. London Spec.

Publ. 334. pp. 163–200.
Ogg, J.G., 2012. Triassic. In: Gradstein, F.M., Ogg, J.G., Schmitz, M.D., Ogg, G.M. (Eds.), The Geologic Time Scale. Elsevier, pp. 681–730. https://doi.org/10.1016/B978-0-444-59425-9.00025-1.
Olsen, P.E., Sues, H.-D., 1986. Correlation of continental Late Triassic and Early Jurassic sediments, and patterns of the Triassic-Jurassic tetrapod transition. In: Padian, K. (Ed.), The Beginning of the Age of Dinosaurs. Cambridge Univ. Press, Cambridge, UK, pp. 321–351.
Olsen, P.E., Shubin, N.H., Anders, M.H., 1987. New Early Jurassic tetrapod assemblages constrain Triassic-Jurassic tetrapod extinction event. Science 237, 1025–1029.
Olsen, P.E., Kent, D.V., Sues, H.-D., Koeberl, C., Huber, H., Montanari, A., Rainforth, E.C., Fowell, S.J., Szajna, M.J., Hartline, B.W., 2002. Ascent of dinosaurs linked to an iridium anomaly at the Triassic-Jurassic boundary. Science 296, 1305–1307.
Onoue, T., Sato, H., Yamashita, D., Ikehara, M., Yasukawa, K., Fujinaga, K., Kato, Y., Matsuoka, A., 2016. Bolide impact triggered the Late Triassic extinction event in equatorial Panthalassa. Sci. Rep. 6, 29609. https://doi.org/10.1038/srep29609.
Onoue, T., Yamashita, K., Fukuda, C., Soda, K., Tomimatsu, Y., Abate, B., Rigo, M., 2018. Sr isotope variations in the Upper Triassic succession at Pizzo Mondello, Sicily: Constraints on the timing of the Cimmerian Orogeny. Palaeogeogr. Palaeoclimatol. Palaeoecol. 499, 131–137.
Orchard, M.J., 2003. Changes on conodont faunas through the Upper Triassic and implications for boundary definitions. In: Geol. Assoc. Canada, Vancouver 2003 meeting. Abs. 28.
Orchard, M.J., 2010. Triassic conodonts and their role in stage boundary definition. In: Lucas, S.G. (Ed.), The Triassic timescale. Geol. Soc. London Publ. 334. pp. 139–161.
Orchard, M.J., Carter, E.S., Lucas, S.G., Taylor, D.G., 2007. Rhaetian (Upper Triassic) condonts and radiolarians from New York Canyon, Nevada, USA. Albertiana 35, 59–65.
Pálfy, J., Demeny, A., Haas, J., Htenyi, M., Orchard, M.J., Veto, I., 2001. Carbon isotope anomaly at the Triassic–Jurassic boundary from a marine section in Hungary. Geology 29, 1047–1050.
Pallister, J.S., Budahn, J.R., Murchey, B.L., 1989. Pillow basalts of the Angayucham Terrane: Oceanic Plateau and Island Crust Accreted to the Brooks Range. J. Geophys. Res. 94, 15901–15923.
Payne, J.L., Lehrmann, D.J., Wei, J.Y., Orchard, M.J., Schrag, D.P., Knoll, A.H., 2004. Large perturbations of the carbon cycle during recovery from the end-Permian extinction. Science 305, 506–509.
Preto, N., Kustatscher, E., Wignall, P.B., 2010. Triassic climates—State of the art and perspectives. Palaeogeogr. Palaeoclimatol. Palaeoecol. 290, 1–10. https://doi.org/10.1016/j.palaeo.2010.03.015.
Preto, N., Rigo, M., Agnini, C., Bertinelli, A., Guaiumi, C., Borello, S., Westphal, H., 2012. Triassic and Jurassic calcareous nannofossils of the Pizzo Mondello section: A SEM study. Riv. Ital. Paleontol. Stratigr. 118, 131–141.
Preto, N., Agnini, C., Rigo, M., Sprovieri, M., Westphal, H., 2013. The calcareous nannofossil *Prinsiosphaera* achieved rock-forming abundances in the latest Triassic of western Tethys: Consequences for the d13C of bulk carbonate. Biogeosciences 10, 6053–6068. https://doi.org/10.5194/bg-10-6053-2013.
Prokoph, A., El Bilali, H., Ernst, R., 2013. Periodicities in the emplacement of large igneous provinces through the Phanerozoic: Relations to ocean chemistry and marine biodiversity evolution. Geosci. Front. 4, 263–276.
Racki, G., Lucas, S.G., 2018. Timing of dicynodont extinction in light of an unusual Late Triassic Polish fauna and Cuvier's approach to extinction. Hist. Biol. https://doi.org/10.1080/08912963.2018.1499734.
Ramezani, J., Bowring, S.A., Pringle, M.S., Winslow III, F.D., Rasbury, E.T., 2005. The Manicouagan impact melt rock: A proposed standard for the intercalibration of U-Pb and 40Ar/39Ar isotopic systems. Geochim. Cosmochim. Acta 69, A321.
Rampino, M.R., Stothers, R.B., 1988. Flood basalt volcanism during the past 250 million years. Science 241, 663–668.
Raup, D.M., Sepkoski, J.J., 1982. Mass extinction in the fossil record. Science 215, 1501–1503. https://doi.org/10.1126/science.215.4539.1501.
Reggiani, L., Bertinelli, A., Ciarapica, G., Marcucci, M., Passeri, L., Ricci, C., Rigo, M., 2005. Triassic–Jurassic stratigraphy of the Madonna del Sirino succession (Lagonegro basin, Southern Apennines, Italy). Boll. Soc. Geol. Ital. 124, 281–291.
Renesto, S., Dalla Vecchia, F.M., 2018. Late Triassic marine reptiles. In: Tanner, L.H. (Ed.), The Late Triassic World. Topics in Geobiology 46 Springer, Cham, pp. 263–313.
Renne, P.R., Balco, G., Ludwig, K.R., Mundil, R., Min, K., 2011. Response to the comment by W.H. Schwarz et al. on "Joint determination of ^{40}K decay constants and $^{40}Ar^{*}/^{40}K$ for the Fish Canyon sanidine standard, and improved accuracy for $^{40}Ar/^{39}Ar$ geochronology" by P.R. Renne et al. (2010). Geochim. Cosmochim. Acta 75, 5097–5100.
Richoz, S., Krystyn, L., Spotl, C., 2007. Towards a carbon isotope reference curve of the Upper Triassic. New Mex. Mus. Nat. Hist. Sci. Bull. 41, 366–367.
Rigo, M., Joachimski, M.M., 2010. Palaeoecology of Late Triassic conodonts: Constraints from oxygen isotopes in biogenic apatite. Acta Palaeontol. Polon. 55, 471–478. https://doi.org/10.4202/app.2009.0100.
Rigo, M., De Zanche, V., Mietto, P., Preto, N., Roghi, G., 2005. Biostratigraphy of the Calcari con Selce formation. Boll. Soc. Geol. Ital. 124, 293–300.
Rigo, M., Preto, N., Roghi, G., Tateo, F., Mietto, P., 2007. A rise in the Carbonate Compensation Depth of western Tethys in the Carnian (Late Triassic). Deep-water evidence for the Carnian Pluvial Event. Palaeogeogr. Palaeoclimatol. Palaeoecol. 246, 188–205. https://doi.org/10.1016/j.palaeo.2006.09.013.
Rigo, M., Trotter, J.A., Preto, N., Williams, I.S., 2012a. Oxygen isotopic evidence for the Late Triassic monsoonal upwelling in the northerwestern Tethys. Geology 40, 515–518.
Rigo, M., Preto, N., Franceschi, M., Guaiumi, C., 2012b. Stratigraphy of the Carnian-Norian Calcari con Selce Formation in the Lagonegro Basin, Southern Apennines. Riv. Ital. Paleontol. Stratigr. 118, 143–154.
Rigo, M., Bertinelli, A., Concheri, G., Gattolin, G., Godfrey, L., Katz, M.E., Maron, M., Muttoni, G., Sprovieri, M., Stellin, F., Zaffani, M., 2016. The Pignola-Abriola section (southern Apennines, Italy): A new GSSP candidate for the base of the Rhaetian Stage. Lethaia 49 (3), 287–306. https://doi.org/10.1111/let.12145.
Rigo, M., Mazza, M., Karádi, V., Nicora, A., 2018. New Upper Triassic conodont biozonation on of the Tethyan Realm. In: Tanner, L.H. (Ed.), The Late Triassic World: Earth in a Time of Transition. Topics in Geobiology 46. pp. 189–235.
Romano, C., Goudemand, N., Vennemann, T.W., Ware, D., Schneebeli-Hermann, E., Hochuli, P.A., Brühwiler, T., Brinkmann, W., Bucher, H., 2013. Climatic and biotic upheavals following the end-Permian mass extinction. Nat. Geosci. 6, 57–60.
Ros, S., 2009. Dinamica de la paleodiversidad de los bivalvos del Triasico y Jurasico inferior. PhD disertacion. Universidad de Valencia, Spain, pp. 563.
Ros, S., Echevarria, J., 2011. Bivalves and evolutionary resilience: Old skills and new strategies to recover from the P/T and T/J extinction events. Hist. Biol. 23, 411–429.
Ros, S., Renzi, M.D., Damborenea, S.E., Marquez-Allianga, A., 2011. Coping between crises: Early Triassic-Early Jurassic bivalve diversity dynamics. Palaeogeogr. Palaeoclimatol. Palaeoecol. 311, 184–199.
Ros, S., Renzi, M.D., Damboranea, S.E., Marquez-Allianga, A., 2012. Part N, revised, volume 1, chapter 25: Early Triassic-Early Jurassic bivalve diversity dynamics. Treatise Online 39, 1–19.
Schaller, M.F., Wright, J.D., Kent, D.V., Olsen, P.E., 2012. Rapid emplacement of the Central Atlantic Magmatic Province as a net sink for CO_2. Earth Planet. Sci. Lett. 323–324, 27–39.
Schmieder, M., Buchner, E., Schwarz, W.H., Trieloff, M., Lambert, P., 2010. A Rhaetian $^{40}Ar/^{39}Ar$ age for the Rochechouart impact structure (France) and implications for the latest Triassic sedimentary record. Meteorit. Planet. Sci. 45, 1225–1242.
Schoene, B., Guex, J., Bartolini, A., Schaltegger, U., Blackburn, T.J., 2010. A correlation between the Triassic–Jurassic boundary mass extinction and flood basalt eruption at the 100-ka level using ID-TIMS U/Pb zircon geochronology. Geology 38, 387–390. https://doi.org/10.1130/G30683.1.
Sephton, M.A., Amor, K., Franchi, I.A., Wignall, P.B., Newton, R., Zonneveld, J.P., 2002. Carbon and nitrogen isotope disturbances and an end-Norian (Late Triassic) extinction event. Geology 30, 1119–1122.
Sepkoski Jr., J.J., 1982. Mass extinctions in the Phanerozoic oceans: A review. Geol. Soc. Am. Spec. Pap. 190, 283–289.
Sepkoski Jr., J.J., 1996. Patterns of Phanerozoic extinctions: A perspective from global databases. In: Walliser, O.H. (Ed.), Global Events and Event Stratigraphy. Springer, Berlin, pp. 35–53.
Seton, M., Mueller, R.D., Zahirovic, S., Gaina, C., Torsvik, T., Shephard, G., Talsma, A., Gurnis, M., Turner, M., Maus, S., Chandler, M., 2012. Global continental and ocean basin reconstructions since 200 Ma. Earth-Sci. Rev. 113, 212–270.
Simms, M.J., Ruffell, A.H., 1989. Synchroneity of climatic change and extinctions in the Late Triassic. Geology 17, 265–268.
Simms, M.J., Ruffell, A.H., 1990. Climatic and biotic change in the Late Triassic. J. Geol. Soc. 147, 321–327.
Simms, M.J., Ruffell, A.H., Johnson, A.L.A., 1995. Biotic and climatic changes in the Carnian (Triassic) of Europe and adjacent areas. In: Fraser, N.C., Sues, H.D. (Eds.), In the Shadow of the Dinosaurs. Early Mesozoic Tetrapods. Cambridge Univ. Press, pp. 352–365.
Spielmann, J.A., Lucas, S.G., Hunt, A.P., 2013. The first Norian (Revueltian) rhynchosaur: Bull Canyon Formation, New Mexico, U.S.A. New Mex. Mus. Nat. Hist. Sci. Bull. 61, 562–566.
Spray, J.G., Thompson, L.M., Biren, M.B., O'Connell-Cooper, C., 2010. The Manicouagan impact structure as a terrestrial analogue site for lunar and Martian planetary science. Planet. Space Sci. 58, 538–551.
Stampfli, G.M., Vavassis, I., De Bono, A., Rosselet, F., Matti, B., Bellini, M., 2003. Remnants of the Paleotethys oceanic suture-zone in the western Tethys area. Boll. Soc. Geol. Ital. Spec. 2, 1–23.
Stanley Jr., George, Shepherd, H.M.E., Robinson, A.J., 2018. Paleoecological response of corals to the End-Triassic mass extinction: An integrational analysis. J. Earth Sci. 29, 879–885.
Sweet, W.C., 1988. The Conodonta. Clarendon Press, New York 212 pp.
Tackett, L.S., Bottjer, D.J., 2016. Paleoecological succession of Norian (Late Triassic) benthic fauna in eastern Panthalassa (Luning and Gabbs formations, west-central Nevada). Palaios 31, 190–202.
Tackett, L.S., Kaufman, A.J., Corsetti, F.A., Bottjer, D.J., 2014. Strontium isotope stratigraphy of the Gabbs Formation (Nevada): implications for global Norian–Rhaetian correlations and faunal turnover. Lethaia 47, 500–511.
Tagle, R., Schmitt, R.T., Erzinger, J., 2009. Identification of the projectile component in the impact structures Rochechouart, France and Sääksjärvi, Finland: Implications for the impactor population for the earth. Geochim. Cosmochim. Acta 73, 4891–4906.
Tanner, L.H., 2010. The Triassic isotope record. In: Lucas, S.G. (Ed.), The Triassic Timescale. Special Publication 334. Geological Society, London, pp. 103–118.
Tanner, L.H., 2018. Climates of the Late Triassic: perspectives, proxies and problems. In: Tanner, L.H. (Ed.), The Late Triassic World: Earth in a Time of Transition. Topics in Geobiology 46. Springer, pp. 59–90.
Tanner, L.H., Lucas, S.G., Chapman, M.G., 2004. Assessing the record and causes of Late Triassic extinctions. Earth-Sci. Rev. 65, 103–139.
Taylor, D.G., Boelling, K., Guex, J., 2000. The Triassic/Jurassic System boundary in the Gabbs Formation, Nevada. In: Hall, R.L., Smith, P.L. (Eds.), Advances in Jurassic Research 2000. Tran Tech Publications Ltd., Zurich, pp. 225–236.
Taylor, D.G., Guex, J., Rakus, M., 2001. Hettangian and Sinemurian ammonoid zonation for the western Cordillera of Noth America. Bull. Geol. Univer. Laus. 350, 381–421.
Teichert, C., 1988. Crises in cephalopod evolution. I. In: Marios, M. (Ed.), L'évolution dans sa Réalité et ses Diverses Modalitées. Fondation Singer-Polignac, Paris, pp. 7–64.
Tintori, A., Lombardo, C., 2018. The Zorzino Limestone actinopterygian fauna from the

Late Triassic (Norian) of the Southern Alps. In: Tanner, L.H. (Ed.), The Late Triassic World: Earth in a Time of Transition. Topics in Geobiology 46. pp. 315–350.
Todaro, S., Di Stefano, P., Zarcone, G., Randazzo, V., 2017. Facies stacking and extinctions across the Triassic–Jurassic boundary in a peritidal succession from western Sicily. Facies 63, 20. https://doi.org/10.1007/s10347-017-0500-5.
Todaro, S., Rigo, M., Randazzo, V., Di Stefano, P., 2018. The end-Triassic mass extinction: A new correlation between extinction events and δ13C fluctuations from a Triassic-Jurassic peritidal succession in western Sicily. Sediment. Geol. 368, 105–113. https://doi.org/10.1016/j.sedgeo.2018.03.008.
Tomašových, A., Siblík, M., 2007. Evaluating compositional turnover of brachiopod communities during the end-Triassic mass extinction (Northern Calcareous Alps): Removal of dominant groups, recovery and community reassembly. Palaeogeogr. Palaeoclimatol. Palaeoecol. 244, 170–200.
Trotter, A.J., Williams, S.I., Nicora, A., Mazza, M., Rigo, M., 2015. Long-term cycles of Triassic climate change: A new d^{18}O record from conodont apatite. Earth Planet. Sci. Lett. 415, 165–174.
Van de Schootbrugge, B., Tremolada, F., Rosenthal, Y., Bailey, T.R., Feist-Burkhardt, S., Brinkhuis, H., Pross, J., Kent, D.V., Falkowski, P.G., 2007. End-Triassic calcification crisis and blooms of organic-walled “disaster species”. Palaeogeogr. Palaeoclimatol. Palaeoecol. 244, 126–141.
Van de Schootbrugge, B., Payne, J.L., Tomasovych, A., Pross, J., Fiebig, J., Benbrahim, M., Follmi, K.B., Quan, T.M., 2008. Carbon cycle perturbation and stabilization in the wake of the Triassic-Jurassic boundary mass extinction event. Geochem. Geophys. Geosyst. 9, 1–16.
van Soest, M.C., Hodges, K.V., Wartho, J.-A., Biren, M.B., Monteleone, B.D., Ramezani, J., Spray, J.G., Thompson, L.M., 2011. (U-Th)/He dating of terrestrial impact structures: The Manicouagan example. Geochem. Geophys. Geosyst. 12, Q0AA16. https://doi.org/10.1029/2010GC003465.
Vazquez, P., Clapham, M.E., 2017. Extinction selectivity among marine fishes during multistressor global change global change in the end-Permian and end-Triassic crises. Geology 45, 395–398.
Veizer, J., Ala, K., Azmy, K., Bruckschen, P., Buhl, D., Bruhn, F., Carden, G.A.F., Diener, A., Ebneth, S., Godderis, Y., Jasper, T., Korte, C., Pawellek, F., Podlaha, O.G., Strauss, H., 1999. $^{87}Sr/^{86}Sr$, $\delta^{13}C$ and $\delta^{18}O$ evolution of Phanerozoic seawater. Chem. Geol. 161, 59–88. https://doi.org/10.1016/S0009-2541(99)00081-9.
Ward, P.D., Haggart, J.W., Carter, E.S., Wilbur, D., Tipper, H.W., Evans, T., 2001. Sudden productivity collapse associated with the Triassic-Jurassic boundary mass extinction. Science 292, 1148–1151.
Ward, P.D., Garrison, G.H., Haggart, J.W., Kring, D.A., Beattie, M.J., 2004. Isotopic evidence bearing on Late Triassic extinction events, Queen Charlotte Islands, British Columbia, and implications for the duration and cause of the Triassic/Jurassic mass extinction. Earth Planet. Sci. Lett. 224, 589–600.
Whiteside, J., Ward, P.D., 2011. Ammonoid diversity and disparity track episodes of chaotic carbon cycling during the early Mesozoic. Geology 39, 99–102.
Whiteside, J.H., Olsen, P.E., Eglinton, T., Brookfield, M.E., Sambrotto, R.N., 2010. Compound-specific carbon isotopes from Earth's largest flood basalt eruptions directly linked to the end-Triassic mass extinction. PNAS 107, 6721–6725.
Wiedmann, J., 1973. Upper Triassic heteromorph ammonites. In: Hallam, A. (Ed.), Atlas of Paleobiogeography. Elsevier, Amsterdam, pp. 235–249.
Wiedmann, J., Kullman, J., 1996. Crises in ammonoid evolution. In: Landman, N. (Ed.), Ammonoid Paleobiology. Topics in Geobiology 13. Springer, pp. 795–813.
Wignall, P.B., 2001. Large igneous provinces and mass extinctions. Earth-Sci. Rev. 53, 1–33.
Wignall, P.B., Zonneveld, J.P., Newton, R.J., Amor, K., Sephton, M.A., Hartley, S., 2007. The end Triassic mass extinction record of Williston Lake, British Columbia. Palaeogeogr. Palaeoclimatol. Palaeoecol. 253, 385–406.
Williford, K.H., Ward, P.D., Garrison, G.H., Buick, R., 2007. An extended organic carbon-isotope record across the Triassic-Jurassic boundary in the Queen Charlotte Islands, British Columbia, Canada. Palaeogeogr. Palaeoclimatol. Palaeoecol. 244, 290–296.
Woodside Energy Ltd, 1977. North Rankin 5. Well Completion Report, Interpretation and Analysis. Government of Western Australia. Department of Mines and Petroleum.
Woodside Energy Ltd, 1981. Delambre 1. Well Completion Report, Interpretation and Analysis. Government of Western Australia. Department of Mines and Petroleum.
Wotzlaw, J.F., Guex, J., Bartolini, A., Gallet, Y., Krystyn, L., McRoberts, C.A., Taylor, D., Schoene, B., Schaltegger, U., 2014. Towards accurate numerical calibration of the Late Triassic: high precision U-Pb geochronology constraints on the duration of the Rhaetian. Geology 42, 571–574.
Zaffani, M., Agnini, C., Concheri, G., Godfrey, L., Katz, M., Maron, M., Rigo, M., 2017. The Norian “chaotic carbon interval”: new clues from the $\delta^{13}C_{org}$ record of the Lagonegro Basin (southern Italy). Geosphere 13 (4), 1–16. https://doi.org/10.1130/GES01459.1.
Zaffani, M., Jadoul, F., Rigo, M., 2018. A new Rhaetian $\delta^{13}C_{org}$ record: Carbon cycle disturbances, volcanism, End-Triassic mass Extinction (ETE). Earth-Sci. Rev. 178, 92–104. https://doi.org/10.1016/j.earscirev.2018.01.004.
Zaninetti, L., Martini, R., Dumont, T., 1992. Triassic foraminifers from sites 761 and 764, Wombat Plateau, northwest Australia. Proc. Ocean Drill. Program Sci. Results 122, 427–436.
Zeng, Z., Zhu, H., Yang, X., Zeng, H., Hu, X., Xia, C., 2019. The Pangaea Megamonsoon records: Evidence from the Triassic Mungaroo Formation, Northwest Shelf of Australia. Gondwana Res. 69, 1–24. https://doi.org/10.1016/j.gr.2018.11.015.